Mathematical Medicine and Biology Page 1 of 35
doi:10.1093/imammb/dqnxxx

A Biochemical and Mechanical Model of Injury-Induced Intimal Thickening

PAK-WING FOK
Ewing Hall 412, Department of Mathematical Sciences,
University of Delaware, Newark, DE 19716.

REBECCA SANFT
Department of Mathematics,
University of North Carolina Asheville,
Asheville, NC 28804.

In this paper, we investigate an axisymmetric model of intimal thickening using hyperelasticity theory. Our model describes growth of the arterial intima due to cell proliferation which in turn is driven by the release of a cytokine such as Platelet-Derived Growth Factor (PDGF). With the growth rate tied to both local stress and the local concentration of PDGF, we derive a quadruple free boundary problem with different regions of the vessel wall characterized by different homeostatic stress. We compare our model predictions to rabbit and rodent models of atherosclerosis and find that in order to achieve the growth rates reported in the experiments, growth must be mainly cytokine-induced rather than stress-induced. Our model is also able to reproduce Glagov remodeling where as a vessel becomes more diseased, the lumen expands before rapidly contracting.

Keywords: Intimal Thickening, Atherosclerosis, Arterial Remodeling, Glagov Remodeling, Hyperelasticity

1. Introduction

Intimal thickening (IT) is a common condition in humans that occurs naturally as a person ages (Aminbakhsh and Mancini, 1999). A healthy blood vessel wall consists of three main layers, of which the innermost is the intima. The intima also includes the endothelium, a single layer of cells that lines the interior of all blood vessels. The surrounding media is composed mainly of smooth muscle cells. The outermost adventitia is composed of connective tissue, containing elastic and collagenous fibers.

IT is distinguished from atherosclerosis since its associated lesions are less inflamed, with macrophages and angiogenic factors notably absent. Nevertheless, IT is related to atherosclerosis because atherosclerotic lesions are thought to arise from thickened intimal cell masses (Kim et al., 1985). In other words, a thickened intima is a precursor to atherosclerosis.

Because of the importance of IT in human atherosclerosis, studies such as Clowes et al. (1983), Stadius et al. (1992) and Jackson et al. (1993) have tried to reproduce similar conditions in animals. One common way to do this is by damaging the arterial endothelium using a balloon catheter. The result is rapid onset of IT, typically occuring over a few months or less. Thickening of the intima is also common after angioplasty operations in humans with accelerated intimal thickening and restenosis occurring in about 30 - 40 % of angioplasty procedures (Hanke et al., 1990). Finally, IT is also manifested in Graft Vascular Disease (GVD), one of the most important and common side-effects of solid organ transplants (Mitchell, 2009). GVD probably arises from general immunologic insult, associated with circulating lymphocytes. Common to all these manifestiations of IT is some kind of injury localized

at, or originating from, the endothelium and subsequent release of cytokines. Injury to the endothelium promotes smooth muscle cell migration from the media, their proliferation in the intima and accelerated intimal thickening. Our goal in this paper is to unify these examples of intimal thickening through a common mathematical model.

Persistent histological changes in the vessel wall are known collectively as remodeling. Released hormones and growth factors are important for controlling vessel wall structure. For example, angiotensin produced by the liver causes vasoconstriction and nitric oxide is a potent vasodilator. Generally, remodeling may or may not be accompanied by an increase in mass but in this paper we use the word to refer to changes in the shape of a vessel that are caused by growth or resorption. For example, the vessels of patients with essential hypertension (Mulvaney, 2002) have encroached lumens: the vessels exhibit inward remodeling. Growth can also cause an outward expansion, or outward remodeling, of the vessel wall. This type of vessel change has been observed in the cerebral veins of pregnant rats (van der Wijk et al., 2013). During intimal thickening, both inward and outward remodeling can be observed (Pasterkamp et al., 1995; Glagov et al., 1987). With our model, we are able to study conditions under which inward and outward remodeling occur and control the spatial distribution of cytokines in the intima to see what effect they have on remodeling.

Broadly, mathematical models for atherosclerosis and its precursors are concerned with both geometric and histological changes to the artery wall. The models can be divided into two types. First, there are studies that attempt to predict properties or constituents of the artery that change in time. For example, Friedman (1989) included smooth muscle cell migration, proliferation, metabolism and other effects to predict the thickening of the intima under shear stress. Hao and Friedman (2014) treated the intima as a porous medium which is coupled to a large system of reaction-diffusion equations for cell and chemical species. They simulated the development of plaque over time by considering a growing (general shaped) domain and created a risk map based on plaque weight, LDL and HDL plasma levels. Ibragimov et al. (2005) and Fok (2011) also used reaction-diffusion PDE models to predict cell and lipid concentrations within a thickened intima, but on a fixed simulation domain. Other researchers such as Ougrinovskaia et al. (2010) treated the buildup of lipid as a dynamical system and studied the steady states using bifurcation theory. Notably absent in these time-evolution models is the prediction of stress and strain profiles due to changes in plaque geometry and/or composition.

Plaques have also been studied from a mechanical perspective by applying finite element analysis to realistic geometries. Bluestein et al. (2008) included fluid interactions to solve for the stress distribution in an eccentric arterial stenosis and to study the effect of microcalcifications on plaque vulnerability. Chau et al. (2004) computed stress and strain distributions based on a geometry obtained from optical coherence tomography and others including Cheng et al. (1993) and Huang et al. (2001) compared the stress distribution in ruptured and stable atherosclerotic lesions to study the effect of calcification on the mechanical stability of plaque. Notably absent in these mechanical models is dynamics: these models cannot predict how plaque geometry or composition evolve over time.

In this paper we propose a model for intimal hyperplasia that describes changes in intima thickness and stress/strain distributions over time, due to growth. It combines the most important aspects of both types of model mentioned above and we believe it is the first model of its kind that describes both changes in stress and cytokine over time. Thus, it is able to illustrate the complex interplay between cytokine-induced growth, stress-induced growth and the spatial distribution of cytokine. The growth process and the cytokine distribution are described by scalar parameters in our model. By comparing the predictions with intima measurements of rabbits and rodents, we find their optimal values using Bayesian inference and Markov Chain Monte Carlo. We find that growth must be driven by cytokine, rather than be stress-induced. Also, in order to reproduce the rapid growth observed in the experiments,

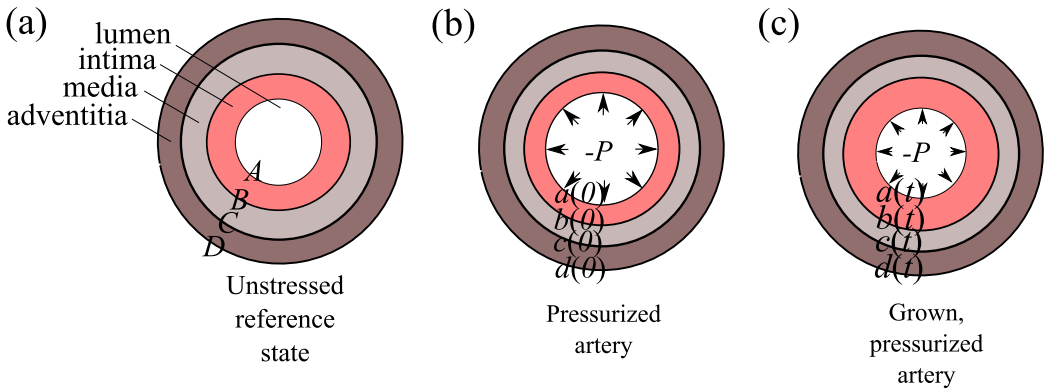

FIG. 1. Geometry in the (a) reference, unstressed configuration when $t < 0$, (b) the pressurized configuration at $t = 0$ and (c) the grown pressurized configuration for $t > 0$. When t, A, B, C, D, a, b, c and d have the hat accent, they are considered dimensional. Otherwise, they are dimensionless.

we predict that the distribution of cytokine must be approximately uniform throughout the intima.

2. Governing Equations

A multiplicative framework to model volumetric growth has been widely used to describe the growth of soft tissue (Ben Amar et al., 2011; Goriely and Ben Amar, 2007; Ambrosi and Mollica, 2002, 2004; Lubarda and Hoger, 2002; Garikipati et al., 2004; Taber and Humphrey, 2001). In our model, all domains are assumed to be axisymmetric. All layers of the vessel wall are assumed to be concentric annuli and remain so for all time $\hat{t}$; see Fig. 1.

Within our framework, the initial configuration is assumed to be stress-free and growth is defined as a change in volume of an unstressed elastic material. At time $\hat{t} = 0$, an internal pressure, P, is applied to the inner wall of the vessel. Then, the vessel grows as a result of the release of growth factors and stress in the system, resulting in a grown, deformed configuration at time $\hat{t} > 0$.

Because our model is based on a multiplicative framework, we introduce notation to describe the arterial vessel wall in a reference unstressed configuration. For time $\hat{t} < 0$, the regions $\hat{A} \leqslant \hat{R} \leqslant \hat{B}$, $\hat{B} \leqslant \hat{R} \leqslant \hat{C}$ and $\hat{C} \leqslant \hat{R} \leqslant \hat{D}$ define the intima, media and adventitia respectively. In the deformed state, the intima, media and adventitia are defined by $\hat{a} \leqslant \hat{r} \leqslant \hat{b}$, $\hat{b} \leqslant \hat{r} \leqslant \hat{c}$ and $\hat{c} \leqslant \hat{r} \leqslant \hat{d}$. Our convention is to use the hat accent for dimensional variables whereas dimensionless variables are unaccented.

2.1 *Diffusion Model for Growth Factors*

Following Fok (2012), we model the development of neointima as being driven by growth factors such as Platelet Derived Growth Factor (PDGF). The release of PDGF comes from platelets, considered to be the "band-aids" of the blood. A paucity of platelets can lead to poor clot formation and increased risk of bleeding, a condition called thrombocytopenia (Patel et al., 2005). Generally, less atherosclerosis is observed in thrombocytopenic rabbits (Stadius et al., 1992). Platelets are derived from megakaryocytes in the marrow and also store other angiogenic payloads such as VEGF (vascular endothelial growth factor), EGF (Epidermal Growth Factor) and IGF (Insulin-like Growth Factor), and our model can be modified to include their effects. However, for simplicity, in this study we will only study a single growth factor

and when the endothelium is injured, we assume platelets adhere to the wound, releasing PDGF (Clowes et al., 1983). PDGF can stimulate the proliferation of smooth muscle cells in the intima and locally induce growth of the tissue. Over long time scales, we may neglect transients so that the distribution of PDGF in the current intimal reference frame $\hat{u}(\hat{r})$ satisfies a steady state diffusion-degradation equation:

$$D_c\left(\frac{1}{\hat{r}}\frac{\partial \hat{u}}{\partial \hat{r}}+\frac{\partial^2 \hat{u}}{\partial \hat{r}^2}\right)-k\hat{u}=0, \qquad \hat{a}\leqslant \hat{r}\leqslant \hat{b}, \tag{2.1}$$

where D_c is the diffusivity for PDGF and k is the natural degradation rate of PDGF. Our boundary conditions are

$$\hat{u}(\hat{a}) = \hat{u}_0 \tag{2.2}$$

$$\left.\frac{\partial \hat{u}}{\partial \hat{r}}\right|_{\hat{r}=\hat{b}} = 0. \tag{2.3}$$

Experimental results on rabbit arteries by Stadius et al. (1992) indicate that during intimal thickening, the media thickness does not change much compared to the intima. The intima and media are separated by a lamina which we assume is impermeable to PDGF. Therefore we assume that diffusive transport of PDGF from the intima into the media is negligible and impose a no-flux boundary condition in (2.3). We assume $\hat{u}(\hat{r})=0$ when $\hat{b}\leqslant\hat{r}\leqslant\hat{d}$ so that there is no growth factor in the media. This is important when we describe the growth tensor in the following section.

2.2 *Wall Mechanics*

In this section we summarize the basic equations of nonlinear elasticity, including the kinematics of deformation, the analysis of stress and the governing equations of equilibrium, and we introduce the constitutive laws for the model.

2.2.1 *Deformation and Decomposition.* We consider a finite deformation in which the cylinder is allowed to grow and deform while remaining cylindrical and we restrict ourselves to radial deformations uniform along the tube axis. Therefore, we focus only on the cross section of the vessel. The deformation is described by the function

$$\hat{r}=\hat{r}(\hat{R}), \qquad \hat{A}\leqslant\hat{R}\leqslant\hat{D}, \tag{2.4}$$

and the deformation gradient tensor, denoted $\mathbf{F}$, in cylindrical coordinates is given by $\mathbf{F}=\mathrm{diag}(\hat{r}'(\hat{R}),\hat{r}/\hat{R},1)$. The tensor $\mathbf{F}$ describes how an infinitesimal line element of material is stretched due to the deformation, and the volume deformation is given by $\det\mathbf{F}$.

Consistent with a morphoelastic theory of growth (Rodriguez et al., 1994), we now assume that the deformation gradient can be decomposed as the product of a growth tensor, $\mathbf{F}_g$ and an elastic tensor, $\mathbf{F}_e$; that is, $\mathbf{F}=\mathbf{F}_e\mathbf{F}_g$. Since growth factors are only present in the intima, we assume the growth tensor takes the form

$$\mathbf{F}_g=\begin{cases}\mathrm{diag}(g,g,1), & \hat{a}\leqslant\hat{r}\leqslant\hat{b},\\ \mathbf{I}, & \hat{b}<\hat{r}\leqslant\hat{d},\end{cases} \tag{2.5}$$

where $g(\hat{r},\hat{t})$ is the (dimensionless) geometric stretch factor associated with growth. and $\mathbf{I}$ is the identity tensor. For modeling simplicity, we assume that the stretch factors in the radial and azimuthal directions are the same. The elastic tensor is given by $\mathbf{F}_e=\mathrm{diag}(\alpha_r,\alpha_\theta,\alpha_z)$ where α_r, α_θ and α_z are geometric

stretch factors in the radial, circumferential and axial directions associated with the elastic deformation. Because we only consider radial deformations along the axis, we always take $\alpha_z = 1$.

The high water content of blood vessels justifies the usual assumption that all three layers of the vessel are incompressible and experimental observations support this assumption (Dobrin and Rovick, 1969; Lawton, 1954). The elastic incompressibility condition $\det\mathbf{F}_e = 1$ implies that $\alpha_\theta \cdot \alpha_r = 1$. Comparing components of $\mathbf{F} = \mathbf{F}_e\mathbf{F}_g$, we find that the elastic stretch factors are

$$\alpha_\theta = \frac{\hat{r}}{\hat{R}g} \equiv \alpha, \qquad \alpha_r = \frac{\hat{R}g}{\hat{r}} \equiv 1/\alpha, \qquad \hat{a} \leqslant \hat{r} \leqslant \hat{b}, \tag{2.6}$$

$$\alpha_\theta = \frac{\hat{r}}{\hat{R}} \equiv \alpha, \qquad \alpha_r = \frac{\hat{R}}{\hat{r}} \equiv 1/\alpha, \qquad \hat{b} < \hat{r} \leqslant \hat{d}. \tag{2.7}$$

The decomposition $\mathbf{F} = \mathbf{F}_e\mathbf{F}_g$ together with the incompressibility condition implies $\det\mathbf{F} = \det\mathbf{F}_g$. Therefore the function $\hat{r}(\hat{R})$ satisfies the ordinary differential equation

$$\begin{gathered} \hat{r}\frac{\partial \hat{r}}{\partial \hat{R}} = \begin{cases} \hat{R}g^2(\hat{r},\hat{t}), & \hat{A} \leqslant \hat{R} \leqslant \hat{B}, \\ \hat{R}, & \hat{B} < \hat{R} \leqslant \hat{D}, \end{cases} \\ \hat{r}(\hat{A}) = \hat{a}. \end{gathered} \tag{2.8}$$

Note that $\hat{r}(\hat{R})$, $\hat{a}$, $\hat{b}$, $\hat{c}$ and $\hat{d}$ all depend on $\hat{t}$ but we omit the explicit dependence to simplify the presentation of the equations. The function $\hat{r}(\hat{R})$ does depend on $\hat{t}$ but only through $g(\hat{r},\hat{t})$ in eq. (2.8). Because $\hat{t}$ only appears explicitly in g and time derivatives do not appear in any of the governing equations, it may be treated as a parameter of the problem. For fixed $\hat{t}$, the solution to eq. (2.8) defines a bijection from $[\hat{a},\hat{b}]$ to $[\hat{A},\hat{B}]$, from $[\hat{b},\hat{c}]$ to $[\hat{B},\hat{C}]$ and from $[\hat{c},\hat{d}]$ to $[\hat{C},\hat{D}]$. If $\hat{a}$ and $g(\hat{r},\hat{t})$ are known, the current configuration is completely determined by the integration of eq. (2.8).

2.2.2 *Stress and Equilibrium.* The surface force per unit area (or stress vector) on an area element is denoted by $\mathbf{t}$ with unit normal $\mathbf{n}$. The stress vector may be expressed as $\mathbf{t} = \hat{\mathbf{T}}^T\mathbf{n}$, where $\hat{\mathbf{T}} = \mathrm{diag}(\hat{T}_{rr}, \hat{T}_{\theta\theta}, \hat{T}_{zz})$ is called the Cauchy stress tensor. Balancing linear momentum ($\mathrm{div}\hat{\mathbf{T}}^T = 0$) and angular momentum ($\hat{\mathbf{T}} = \hat{\mathbf{T}}^T$) , the mechanical equilibrium equation becomes

$$\mathrm{div}\hat{\mathbf{T}} = 0. \tag{2.9}$$

Assuming the material is incompressible, the Cauchy stress $\hat{\mathbf{T}}$ in the intima and media/adventitia, is related to the elastic deformation, $\mathbf{F}_e$, by

$$\hat{\mathbf{T}} = \mathbf{F}_e \frac{\partial W}{\partial \mathbf{F}_e} - p\mathbf{I}, \tag{2.10}$$

where p is a Lagrange multiplier associated with the internal constraint of incompressibility, and $W = W_1, W_2, W_3$ is the strain energy function describing the intima, media and adventita respectively. Equations (2.9,2.10), and the incompressibility constraint $\det\mathbf{F_e} = 1$ provide four equations to solve for $\hat{r}(\hat{R},\hat{t})$, $\hat{T}_{rr}$, $\hat{T}_{\theta\theta}$ and p.

2.2.3 *Elastic Response* We assume that the body is hyperelastic and therefore the material can be described by a strain energy function $W = W(\mathbf{F}_e)$. For the intima, we use a neo-Hookean strain energy density function to describe the material:

$$W_1(I_1) = \mu_1(I_1 - 3), \tag{2.11}$$

where $I_1 = \alpha_r^2 + \alpha_\theta^2 + \alpha_z^2$ is an invariant of the right Cauchy-Green tensor $\mathbf{C} = \mathbf{F}_e^T \mathbf{F}_e$. Using Equation (2.6), $I_1 = \alpha^{-2} + \alpha^2 + 1$. While the stiffness of human plaques in their late stages have been measured by many authors such as Lee et al. (1992); Barrett et al. (2009), Baldewsing et al. (2004) and Born and Richardson (1990), layer specific studies are rarer. Generally, there are few studies that measure μ_1 and even fewer studies that measure μ_1 for non-human organisms (in this paper we are primarily interested in the intima growth of rabbits and rodents). Holzapfel et al. (2005) have measured μ_1 in humans, but its value varies greatly from sample to sample. In tables 1 and 2, we estimate $\mu_1 = 20$ kPa but for later results, consider a range of values for μ_1.

For the media and adventitia, many authors such as Gasser et al. (2006), Akyildiz et al. (2011), Badel et al. (2011) and Holzapfel (2000) adopt exponential-type strain energy functions. We follow Holzapfel (2000) and Badel et al. (2011) and adopt a form

$$W_k(I_1, I_4) = \mu_k(I_1 - 3) + \frac{\eta_k}{\beta_k}\left(e^{\beta_k (I_4^{(k)} - 1)^2} - 1\right), \qquad k = 2, 3, \tag{2.12}$$

$$I_4^{(k)} = \alpha_\theta^2 \cos^2\varphi_k + \alpha_z^2 \sin^2\varphi_k = \alpha^2 \cos^2\varphi_k + \sin^2\varphi_k, \tag{2.13}$$

representing the media ($k = 2$) and adventitia ($k = 3$). Anisotropy in (2.12) arises due to the presence of embedded collagen fibers aligned tangentially to the surface of the tissue and is manifested through the dependence on the invariant $I_4^{(k)}$, with $2\varphi_k$ being the angle between these fibers: at large strains, the medial and adventitial layers become stiffer due to their presence. Note that the material properties of the media and adventitia are layer-specific and characterized by the 4 parameters $(\mu_2, \eta_2, \beta_2, \varphi_2)$ and $(\mu_3, \eta_3, \beta_3, \varphi_3)$ respectively. Their values are taken from Holzapfel (2000) and Badel et al. (2011) and are summarized in Tables 1 and 2 for both rabbits and rodents, two animals where intima hyperplasia has been experimentally characterized in considerable detail.

Symbol	Meaning	Value	Reference/Notes
μ_1	intima material constant	20 kPa	Estimated
μ_2	media material constant	1.5 kPa	Holzapfel (2000)
η_2	media material constant	2.36 kPa	Holzapfel (2000)
β_2	media material constant	0.83	Holzapfel (2000)
φ_2	media fiber angle	29.0°	Holzapfel (2000)
μ_3	adventitia material constant	0.15 kPa	Holzapfel (2000)
η_3	adventitia material constant	0.56 kPa	Holzapfel (2000)
β_3	adventitia material constant	0.71	Holzapfel (2000)
φ_3	adventitia fiber angle	62.0°	Holzapfel (2000)
$\hat{A}$	lumen radius	1 mm	Stadius et al. (1992)
$\hat{B}$	internal elastic lamina radius	1.001 mm	Estimated
$\hat{C}$	external elastic lamina radius	1.06 mm	Stadius et al. (1992)
$\hat{D}$	vessel radius	1.110 mm	Stadius et al. (1992)
τ	Duration of experiment	45 days	Stadius et al. (1992)
D_c	PDGF diffusivity	-	Free parameter
k	PDGF degradation rate	-	Free parameter
P	arterial pressure	100 mmHg	Estimated

Table 1. Model parameters for a rabbit carotid artery. PDGF = Platelet Derived Growth Factor.

Symbol	Meaning	Value	Reference/Notes
μ_1	intima material constant	20 kPa	Estimated
μ_2	media material constant	4.4 kPa	Badel et al. (2011)
η_2	media material constant	13.9 kPa	Badel et al. (2011)
β_2	media material constant	21.6	Badel et al. (2011)
φ_2	media fiber angle	41.9°	Badel et al. (2011)
μ_3	adventitia material constant	4.4 kPa	Badel et al. (2011)
η_3	adventitia material constant	11.8 kPa	Badel et al. (2011)
β_3	adventitia material constant	0.242	Badel et al. (2011)
φ_3	adventitia fiber angle	5.14°	Badel et al. (2011)
$\hat{A}$	lumen radius	0.38 mm	Clowes et al. (1983)
$\hat{B}$	internal elastic lamina radius	0.3805 mm	Estimated
$\hat{C}$	external elastic lamina radius	0.42 mm	Clowes et al. (1983)
$\hat{D}$	vessel radius	0.45 mm	Clowes et al. (1983)
τ	Duration of experiment	14 weeks	Clowes et al. (1983)
D_c	PDGF diffusivity	-	Free parameter
k	PDGF degradation rate	-	Free parameter
P	arterial pressure	120 mmHg	Estimated

Table 2. Model parameters for a rodent carotid artery. PDGF = Platelet Derived Growth Factor.

2.2.4 *Finite Deformation.* The only non-vanishing component of the mechanical equilibrium equation $\mathrm{div}\hat{\mathbf{T}} = 0$, is

$$\frac{\partial \hat{T}_{rr}}{\partial \hat{r}} + \frac{\hat{T}_{rr} - \hat{T}_{\theta\theta}}{\hat{r}} = 0, \tag{2.14}$$

where $\hat{T}_{rr}$ and $\hat{T}_{\theta\theta}$ are the radial and hoop Cauchy stresses. Introducing the auxiliary functions $\omega_k(\alpha) = W_k(\alpha^{-1}, \alpha)$ for $k = 1,2,3$, eqs. (2.11) and (2.12) imply that

$$\begin{aligned}
\omega_1(\alpha) &= \mu_1(\alpha^2 + \alpha^{-2} - 2), \\
\omega_2(\alpha) &= \mu_2(\alpha^2 + \alpha^{-2} - 2) + \frac{\eta_2}{\beta_2}\left(e^{\beta_2(\alpha^2\cos^2\varphi_2 + \sin^2\varphi_2 - 1)^2} - 1\right), \\
\omega_3(\alpha) &= \mu_3(\alpha^2 + \alpha^{-2} - 2) + \frac{\eta_3}{\beta_3}\left(e^{\beta_3(\alpha^2\cos^2\varphi_3 + \sin^2\varphi_3 - 1)^2} - 1\right).
\end{aligned} \tag{2.15}$$

The stress-strain relationship in (2.10) can be used in eq. (2.14) to obtain

$$\frac{\partial \hat{T}_{rr}(\hat{r})}{\partial \hat{r}} = \begin{cases} \dfrac{\alpha}{\hat{r}}\dfrac{\partial \omega_1}{\partial \alpha}, & \hat{a} \leqslant \hat{r} \leqslant \hat{b}, \\ \dfrac{\alpha}{\hat{r}}\dfrac{\partial \omega_2}{\partial \alpha}, & \hat{b} \leqslant \hat{r} \leqslant \hat{c}, \\ \dfrac{\alpha}{\hat{r}}\dfrac{\partial \omega_3}{\partial \alpha}, & \hat{c} \leqslant \hat{r} \leqslant \hat{d}, \end{cases} \tag{2.16}$$

where α in the intima $\hat{a} \leqslant \hat{r} \leqslant \hat{b}$, media $\hat{b} < \hat{r} \leqslant \hat{c}$ and adventitia $\hat{c} \leqslant \hat{r} \leqslant \hat{d}$ are given by (2.6) and (2.7) respectively. We assume an internal pressure, P, at the inner boundary so that $\hat{T}_{rr}(\hat{r} = \hat{a}) = -P$.

The form of the outer boundary condition depends on the presence of perivascular tissue. Although its effect on the adventitia is unclear at the moment, we refer to Masson et al. (2008) for some preliminary studies. In our model for simplicity, we assume zero traction on the outer boundary: $\hat{T}_{rr}(\hat{r}=\hat{d})=0$. Using these boundary conditions, we integrate equation (2.16) to obtain the radial stress as

$$\hat{T}_{rr}(\hat{r}) = \begin{cases} -P+\eta_2\displaystyle\int_{\hat{a}}^{\hat{r}} \alpha^2(\hat{r}')Q_1[\alpha(\hat{r}')]\frac{\mathrm{d}\hat{r}'}{\hat{r}'}, & \hat{a}\leqslant\hat{r}\leqslant\hat{b}, \\ -\eta_2\displaystyle\int_{\hat{c}}^{\hat{d}} \alpha^2(\hat{r}')Q_3[\alpha(\hat{r}')]\frac{\mathrm{d}\hat{r}'}{\hat{r}'}-\eta_2\int_{\hat{r}}^{\hat{c}} \alpha^2(\hat{r}')Q_2[\alpha(\hat{r}')]\frac{\mathrm{d}\hat{r}'}{\hat{r}'}, & \hat{b}\leqslant\hat{r}\leqslant\hat{c}, \\ -\eta_2\displaystyle\int_{\hat{r}}^{\hat{d}} \alpha^2(\hat{r}')Q_3[\alpha(\hat{r}')]\frac{\mathrm{d}\hat{r}'}{\hat{r}'}, & \hat{c}\leqslant\hat{r}\leqslant\hat{d}, \end{cases} \tag{2.17}$$

where $Q_j[\alpha]$, $j=1,2,3$ are

$$Q_1[\alpha] = \frac{2\mu_1}{\eta_2}\left(1-\alpha^{-4}\right), \tag{2.18}$$

$$Q_2[\alpha] = \frac{2\mu_2}{\eta_2}(1-\alpha^{-4})+4\cos^2\varphi_2(\alpha^2\cos^2\varphi_2+\sin^2\varphi_2-1)e^{\beta_2(\alpha^2\cos^2\varphi_2+\sin^2\varphi_2-1)^2}, \tag{2.19}$$

$$Q_3[\alpha] = \frac{2\mu_3}{\eta_2}(1-\alpha^{-4})+\frac{4\eta_3}{\eta_2}\cos^2\varphi_3(\alpha^2\cos^2\varphi_3+\sin^2\varphi_3-1)e^{\beta_3(\alpha^2\cos^2\varphi_3+\sin^2\varphi_3-1)^2}. \tag{2.20}$$

The hoop stress is then given by $\hat{T}_{\theta\theta}=\hat{r}\frac{\partial\hat{T}_{rr}}{\partial\hat{r}}+\hat{T}_{rr}$:

$$\hat{T}_{\theta\theta}(\hat{r}) = \hat{T}_{rr}+\begin{cases} \eta_2\alpha^2(\hat{r})Q_1[\alpha(\hat{r})], & \hat{a}\leqslant\hat{r}\leqslant\hat{b} \\ \eta_2\alpha^2(\hat{r})Q_2[\alpha(\hat{r})], & \hat{b}<\hat{r}\leqslant\hat{c}, \\ \eta_2\alpha^2(\hat{r})Q_3[\alpha(\hat{r})], & \hat{c}<\hat{r}\leqslant\hat{d}, \end{cases} \tag{2.21}$$

where we have used (2.14) and (2.16). The inner boundary, $\hat{a}$, is determined by the boundary conditions at the interfaces of the three layers. At the surfaces of stress discontinuity $\hat{r}=\hat{b}$ and $\hat{r}=\hat{c}$, the associated traction needs to be equal but opposite, which requires the radial stress to be continuous across $\hat{r}$, that is

$$\hat{T}_{rr}(\hat{b}^+)=\hat{T}_{rr}(\hat{b}^-) \quad\Rightarrow\quad -\frac{P}{\eta_2}+\int_{\hat{a}}^{\hat{b}}\alpha^2(\hat{r}')Q_1[\alpha(\hat{r}')]\frac{\mathrm{d}\hat{r}'}{\hat{r}'}=\frac{\hat{T}_{rr}(\hat{c})}{\eta_2}-\int_{\hat{b}}^{\hat{c}}\alpha^2(\hat{r}')Q_2[\alpha(\hat{r}')]\frac{\mathrm{d}\hat{r}'}{\hat{r}'} \tag{2.22}$$

$$\hat{T}_{rr}(\hat{c}^+)=\hat{T}_{rr}(\hat{c}^-) \quad\Rightarrow\quad \frac{\hat{T}_{rr}(\hat{c})}{\eta_2}=-\int_{\hat{c}}^{\hat{d}}\alpha^2(\hat{r}')Q_3[\alpha(\hat{r}')]\frac{\mathrm{d}\hat{r}'}{\hat{r}'}. \tag{2.23}$$

Since there is always a one-to-one correspondence between the reference and current configurations, eq. (2.22) and eq. (2.23) can be recast in terms of the reference radial coordinate $\hat{R}$. In addition, the expression for $\hat{T}_{rr}(\hat{c})$ in eq. (2.23) can be used in eq. (2.22):

$$-\frac{P}{\eta_2}+\int_{\hat{A}}^{\hat{B}}Q_1[\alpha(\hat{R})]\frac{\mathrm{d}\hat{R}}{\hat{R}}+\int_{\hat{B}}^{\hat{C}}Q_2[\alpha(\hat{R})]\frac{\mathrm{d}\hat{R}}{\hat{R}}+\int_{\hat{C}}^{\hat{D}}Q_3[\alpha(\hat{R})]\frac{\mathrm{d}\hat{R}}{\hat{R}}=0. \tag{2.24}$$

2.2.5 *Growth Function.* The equations above need to be supplemented with a specific form for the function $g(\hat{r},\hat{t})$ in (2.5). Through conservation of mass, one can show that the growth tensor $\mathbf{F}_g$ is related

to the growth rate Γ through the relationship $\mathrm{tr}(\mathbf{F}_g^{-1}\dot{\mathbf{F}}_g) = \Gamma$ (Ben Amar et al., 2011). This is the tensor generalization of the "natural" definition for growth rate in terms of scalar stretch factors $\Gamma = \dot{F}_g/F_g$. It follows that the growth rate Γ for the intima is given by $\Gamma = \frac{2}{g}\frac{\partial g}{\partial \hat{t}}$ with initial condition $g(0) = 1$. Solving for g, we find that

$$g(\hat{r},\hat{t}) = \exp\left\{\frac{1}{2}\int_0^{\hat{t}} \Gamma(\hat{r},\hat{t}')d\hat{t}'\right\}. \tag{2.25}$$

Although g is the geometric stretch due to growth, for simplicity, we will refer to g in (2.25) simply as the *growth function*. Eq. (2.25) states that the growth function at time $\hat{t}$ depends on the history of the growth rate Γ up to time $\hat{t}$. However, implementing (2.25) in our model is computationally intensive and so for simplicity, we use instead the approximation

$$g(\hat{r},\hat{t}) \approx \exp\left\{\frac{\Gamma(\hat{r},\hat{t})\hat{t}}{2}\right\}. \tag{2.26}$$

We checked that using (2.26) instead of (2.25) does not change the qualitative nature of the vessel evolution.

The form of the biomechanical growth law associated with Γ is a topic of ongoing research. Studies such as Taber (1995) and Luo et al. (1995) have proposed growth and remodeling laws for bone and soft tissues that depend on stress, strain rate, and strain-energy density. Many experimental studies such as Ueba et al. (1997) and Sterpetti et al. (1993) show that smooth muscle cells are sensitive to the magnitude of local stress and may show smaller or larger proliferation rates accordingly. Volokh (2006) shows that circumferential stresses can be larger than the radial stress by an order of magnitude and play a significant role in cell proliferation. In particular, Wayman et al. (2008) show that smooth muscle cell proliferation is significantly greater at high circumferential stress. In light of these studies, we assume that the growth rate is proportional to deviations from some homeostatic circumferential stress $\tilde{T}_{\theta\theta}$:

$$\Gamma(\hat{r},\hat{t}) \quad = \quad \zeta(\hat{T}_{\theta\theta} - \tilde{T}_{\theta\theta}(\hat{r},\hat{u})), \tag{2.27}$$

where $\zeta > 0$ has units of (time $\times$ stress)$^{-1}$. Because the presence of PDGF is known to increase cell proliferation rate (Yu et al., 2003) and regulate the homeostatic environment of cells (Heuchel et al., 1999), we have allowed $\tilde{T}_{\theta\theta}$ in (2.27) to depend on the local PDGF concentration. Another interpretation of (2.27) is that PDGF modulates the local homeostatic stress. Different parts of the vessel wall experience a different homeostatic stress depending on the local concentration of cytokine and vessel wall tissue grows in order to achieve its local "desired" homeostatic stress state. Eq. (2.27) also allows for resorption which could arise from the effects of enzymes or a net decrease in smooth muscle cell population.

For a fixed stress $\hat{T}_{\theta\theta}$ and position $\hat{r}$, the growth rate should increase with PDGF concentration, implying that $\partial\tilde{T}_{\theta\theta}/\partial\hat{u} < 0$: see Fig. 2. The experiments of Sterpetti et al. (1993) on bovine arterial SMCs indicate that PDGF may also be released by cells under stress, but strictly speaking, this is neglected in our model where the only source of PDGF is from platelets that adhere to the endothelium. However, we can qualitatively mimic the effect of PDGF-mediated bulk growth by taking $kL^2/D_c \ll 1$ where L is a baseline, or typical intimal thickness. In this limit, PDGF degrades very slowly so that the entire intima is saturated with PDGF and undergoes a bulk growth.

Finally we note that there are two time scales to this problem: one associated with growth ("slow") and one associated with relaxation of stresses and cytokines ("fast"). By assuming that stresses and cytokine concentrations relax much more quickly compared to the evolution of the geometric domain (the

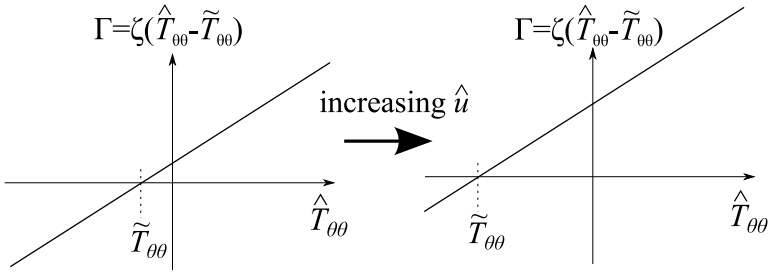

FIG. 2. The range of stresses $\hat{T}_{\theta\theta}$ that results in a positive growth rate increases with increasing PDGF concentration $\hat{u}$. Equivalently, the homeostatic stress $\tilde{T}_{\theta\theta}$ is a decreasing function of $\hat{u}$.

adiabatic or quasi-steady approximation), we solve the steady-state equations (2.14) and (2.1) instead of their fully time-dependent counterparts. Nevertheless, $\hat{T}_{\theta\theta} = \hat{T}_{\theta\theta}(\hat{r},\hat{t})$ in eq. (2.27) evolves on the "slow" time scale and is a function of $\hat{t}$ because the domain $\hat{a}(\hat{t}) \leqslant \hat{r} \leqslant \hat{d}(\hat{t})$ also evolves on the slow time scale.

3. Non-dimensionalization

We introduce dimensionless variables

$$
\begin{aligned}
u &= \hat{u}/u_0, && (3.1)\\
r &= \hat{r}/L, \qquad L = \hat{D} - \hat{A}, && (3.2)\\
R &= \hat{R}/L, && (3.3)\\
A &= \hat{A}/L, \qquad a = \hat{a}/L, && (3.4)\\
B &= \hat{B}/L, \qquad b = \hat{b}/L, && (3.5)\\
C &= \hat{C}/L, \qquad c = \hat{c}/L, && (3.6)\\
D &= \hat{D}/L, \qquad d = \hat{d}/L, && (3.7)\\
t &= \hat{t}/\tau, && (3.8)\\
\mathbf{T} &= \hat{\mathbf{T}}/\eta_2, && (3.9)
\end{aligned}
$$

where τ is the timescale associated with hyperplasia, which could be on the order of weeks for the denudation experiments in animals but years for angioplasty or GVD-induced IT in humans. We have rescaled the variables so that the thickness of the undeformed intima-media-adventitia composite layer is 1 and used η_2 as a reference stress.

The diffusion-degradation equation in eq. (2.1) is non-dimensionalized, and we find that the distribution of PDGF satisfies

$$r^2 u''(r) + r u'(r) - \lambda^2 r^2 u = 0, \qquad \lambda = \sqrt{kL^2/D_c}, \tag{3.10}$$

with boundary conditions

$$u(a) = 1, \tag{3.11}$$
$$u'(b) = 0, \tag{3.12}$$

where the prime denotes a derivative with respect to r. With these boundary conditions, the solution to (3.10) is

$$u(r) = \frac{K_1(\lambda b)I_0(\lambda r) + I_1(\lambda b)K_0(\lambda r)}{I_1(\lambda b)K_0(\lambda a) + I_0(\lambda a)K_1(\lambda b)}, \tag{3.13}$$

where $I_j(\cdot)$ and $K_j(\cdot)$ are modified Bessel functions of the first and second kind. Because D_c and k are free parameters in our model, λ in eq. (3.10) is treated as a free dimensionless parameter. The mapping from the reference frame to the current frame satisfies the ODE

$$\frac{dr}{dR} = \begin{cases} Rg^2(r,t;a,b)/r, & A \leqslant R \leqslant B, \\ R/r, & B < R \leqslant D, \end{cases} \tag{3.14}$$

subject to the initial condition

$$r(A) = a. \tag{3.15}$$

Now we non-dimensionalize the growth function g; see eqs. (2.26) and (2.27). What is the functional form of the homeostatic stress $\tilde{T}_{\theta\theta}(\hat{r},\hat{u})$? In this paper, we take

$$\tilde{T}_{\theta\theta}(\hat{r},\hat{u}) = G_1(\hat{r}) + G_2\hat{u}, \tag{3.16}$$

where $G_2 < 0$ is a negative constant since $\frac{\partial \tilde{T}_{\theta\theta}}{\partial \hat{u}} < 0$. This form of $\tilde{T}_{\theta\theta}$ has desirable biological and mathematical properties. Substituting (3.16) into (2.27), we have

$$\Gamma\tau = \nu_1(T_{\theta\theta} - \bar{T}_{\theta\theta}(r)) + \nu_2 u, \tag{3.17}$$

where we define

$$\nu_1 = \eta_2\zeta\tau, \qquad \nu_2 = -\zeta u_0 \tau G_2, \qquad \bar{T}_{\theta\theta}(r) = \frac{G_1(\hat{r})}{\eta_2}, \tag{3.18}$$

as dimensionless parameters and $\nu_1, \nu_2 > 0$. Both ν_1 and ν_2 are treated as free parameters in our model. Note that $\tilde{T}_{\theta\theta}(\hat{r},0) = G_1(\hat{r})$ in eq. (3.16) is the homeostatic hoop stress in the absence of PDGF. We identify $\nu_1(T_{\theta\theta} - \bar{T}_{\theta\theta})$ as the contribution to the growth rate due to local stress and $\nu_2 u$ as the contribution to the growth rate due to the presence of PDGF. Furthermore, when the local stress is identical to this baseline homeostatic stress, the growth rate is just proportional to the PDGF concentration. One would certainly expect this to be true for low concentrations and Hill-type saturation effects can also be modeled by appropriate modification of eq. (3.16).

The full growth function is

$$g(r,t,\mathbf{T}) = \exp\left[\frac{\nu_1 t(T_{\theta\theta} - \bar{T}_{\theta\theta}(r))}{2}\right] \times \exp\left[\frac{\nu_2 t}{2} \times \underbrace{\frac{I_1(\lambda b)K_0(\lambda r) + K_1(\lambda b)I_0(\lambda r)}{I_1(\lambda b)K_0(\lambda a) + I_0(\lambda a)K_1(\lambda b)}}_{u}\right], \tag{3.19}$$

so that at a fixed time t, the magnitude of g changes with r. In particular, when $\nu_1 = 0, \nu_2 > 0$, g decreases with r because the PDGF concentration u decreases away from the endothelium at $r = a$. By

assuming that $\tilde{T}_{\theta\theta}$ has an additive structure in eq. (3.16), we see that the growth function (3.19) has a multiplicative dependence on PDGF concentration and deviation from baseline homeostatic stress.

Another benefit of assuming eq. (3.16) is that $\bar{T}_{\theta\theta}(r)$ in (3.17) is simple to calculate and is intuitively easy to understand. When there is no injury and no release of PDGF ($u = 0$), the growth rate should be zero, the pressurized vessel should be in mechanical equilibrium and $g = 1$. Therefore, the resulting hoop stress in the pressurized vessel must be identical to the homeostatic hoop stress $\bar{T}_{\theta\theta}(r)$. The calculation of $\bar{T}_{\theta\theta}(r)$ initializes our algorithm to simulate intimal thickening and details can be found in the appendix.

Now we dimensionalize eq. (2.24) to find

$$-\frac{P}{\eta_2}+\int_C^D \frac{Q_3[\alpha(R)]\mathrm{d}R}{R}+\int_A^B \frac{Q_1[\alpha(R)]\mathrm{d}R}{R}+\int_B^C \frac{Q_2[\alpha(R)]\mathrm{d}R}{R}=0, \tag{3.20}$$

where the elastic deformation viewed from the reference frame is

$$\alpha(R,t;a,b)=\begin{cases} \dfrac{r(R)}{Rg[r(R),t;a,b]}, & A\leqslant R\leqslant B,\\[2ex] \dfrac{r(R)}{R}, & B<R\leqslant D, \end{cases} \tag{3.21}$$

while the elastic deformation viewed from the current configuration is

$$\alpha(r,t;a,b)=\begin{cases} \dfrac{r}{R(r)g[r,t;a,b]}, & a\leqslant r\leqslant b,\\[2ex] \dfrac{r}{R(r)}, & b<r\leqslant d. \end{cases} \tag{3.22}$$

As a shorthand, we have used α for both types of deformation and they are distinguished by their arguments. The dimensionless radial and hoop stresses are

$$T_{rr}(r)=\begin{cases} -\dfrac{P}{\eta_2}+\displaystyle\int_a^r \alpha^2(r')Q_1[\alpha(r')]\frac{\mathrm{d}r'}{r'}, & a\leqslant r\leqslant b,\\[2ex] -\displaystyle\int_c^d \alpha^2(r')Q_3[\alpha(r')]\frac{\mathrm{d}r'}{r'}-\int_r^c \alpha^2(r')Q_2[\alpha(r')]\frac{\mathrm{d}r'}{r'}, & b\leqslant r\leqslant c,\\[2ex] -\displaystyle\int_r^d \alpha^2(r')Q_3[\alpha(r')]\frac{\mathrm{d}r'}{r'}, & c\leqslant r\leqslant d, \end{cases} \tag{3.23}$$

$$T_{\theta\theta}(r)=T_{rr}(r)+\begin{cases} \alpha^2(r)Q_1[\alpha(r)] & a\leqslant r\leqslant b,\\ \alpha^2(r)Q_2[\alpha(r)], & b<r\leqslant c,\\ \alpha^2(r)Q_3[\alpha(r)], & c<r\leqslant d. \end{cases} \tag{3.24}$$

4. Validation study

The solution to our model at a fixed t involves the four unknown boundaries $a(t)$, $b(t)$, $c(t)$, $d(t)$ and the six unknown functions $T_{rr}(r,t)$, $T_{\theta\theta}(r,t)$, $\alpha(r,t)$, $g(r,t)$, $\Gamma(r,t)$ and $u(r,t)$ (although $\Gamma(r,t)$ is easily derived from $g(r,t)$ and u is calculated from eq. (3.13)). When $t = 0$, $g = 1$ and the base homeostatic stress

$\bar{T}_{\theta\theta}$ is calculated as the hoop stress response to the applied internal pressure P. We find these quantities by solving eqs. (3.10)-(3.15) and eqs. (3.19)-(3.24) for a given t and an appropriate discretization of $[a,d]$. The result is a large set of algebraic equations which can be solved at each t using Newton's method. More details are given in Appendix A.

To check that our numerical method performs correctly, we find an asymptotic solution to (3.10)-(3.15) in the case when $P = \lambda = 0$, valid when $t = \delta t \ll 1$. These solutions are given below, and their derivation is discussed in Appendix B.

$$\begin{aligned}
\delta T_{\theta\theta}(R) &\sim -\frac{\nu_2\delta t}{4\Delta}\left(1+\frac{A^2}{R^2}\right)B^2Q_1'[1]\left(C^2D^2Q_2'[1]+B^2D^2(Q_3'[1]-Q_2'[1])-B^2C^2Q_3'[1]\right),\\
\delta r(R) &\sim \frac{\nu_2\delta t}{2\Delta}\left(A^2C^2D^2(Q_2'[1]-Q_1'[1])R+A^2B^2D^2(Q_3'[1]-Q_2'[1])R-B^2C^2(A^2Q_3'[1]-D^2Q_1'[1])R\right.\\
&\quad \left.-A^2B^4D^2(Q_3'[1]-Q_2'[1])R^{-1}+A^2B^2C^2(B^2Q_3'[1]-D^2Q_2'[1])R^{-1}\right),\\
\delta a(t) &\sim -\frac{\nu_2\delta t}{2\Delta}A(B^2-A^2)\left(B^2D^2(Q_3'[1]-Q_2'[1])+C^2D^2(Q_2'[1]-Q_1'[1])-B^2C^2Q_3'[1]\right), \qquad (4.1)\\
\delta b(t) &\sim \frac{\nu_2\delta t}{2\Delta}B(B^2-A^2)C^2D^2Q_1'[1],\\
\delta c(t) &\sim \frac{\nu_2\delta t}{2\Delta}C(B^2-A^2)B^2D^2Q_1'[1],\\
\delta d(t) &\sim \frac{\nu_2\delta t}{2\Delta}D(B^2-A^2)B^2C^2Q_1'[1].
\end{aligned}$$

for $0 \leqslant \delta t \ll 1$, where

$$\Delta = B^2C^2D^2Q_1'[1]+A^2B^2D^2(Q_3'[1]-Q_2'[1])+A^2C^2D^2(Q_2'[1]-Q_1'[1])-Q_3'[1]A^2B^2 \qquad (4.2)$$

and $Q_1'[1] = \frac{8\mu_1}{\eta_2}$, $Q_2'[1] = 8\left(\frac{\mu_2}{\eta_2}+\cos^4\varphi_2\right)$ and $Q_3'[1] = 8\left(\frac{\mu_3}{\eta_2}+\cos^4\varphi_3\right)$. In Figure 3, we see that the full computational solution and the asymptotic solution (4.1) match well with each other for small times.

5. Results

There are three main factors that give rise to rich and interesting behaviors for our model. First, the growth depends on both local stress and cytokine concentration. Released growth factors stimulate growth within the intima which modulates the local stress. The stress in turn feeds back into the growth function.

Second, the growth is non-uniform within the intima: it is generally larger near the lumen and smaller near the media. By making $\lambda \gg 1$, we can localize growth factor near the lumen. The other extreme is when $\lambda \ll 1$. This corresponds to a long half-life for the growth factor so that it is present at high concentrations throughout the entire intima. The two limits give rise to qualitatively different evolutions, as we will discuss later. A similar phenomenon is seen in spherical tumors (Ben Amar et al., 2011) that are fed by nutrients. Initially, the tumor undergoes exponential growth since all cells in the tumor have access to high levels of nutrient. As the tumor grows, high levels of nutrients are present in only the outermost "shell" of cells and the growth transitions from exponential to linear.

Third, the media thins as it deforms in order to conserve mass. A further complication is that both the intima and media stiffen as they deform and interesting dynamics arises due to competing stiffnesses.

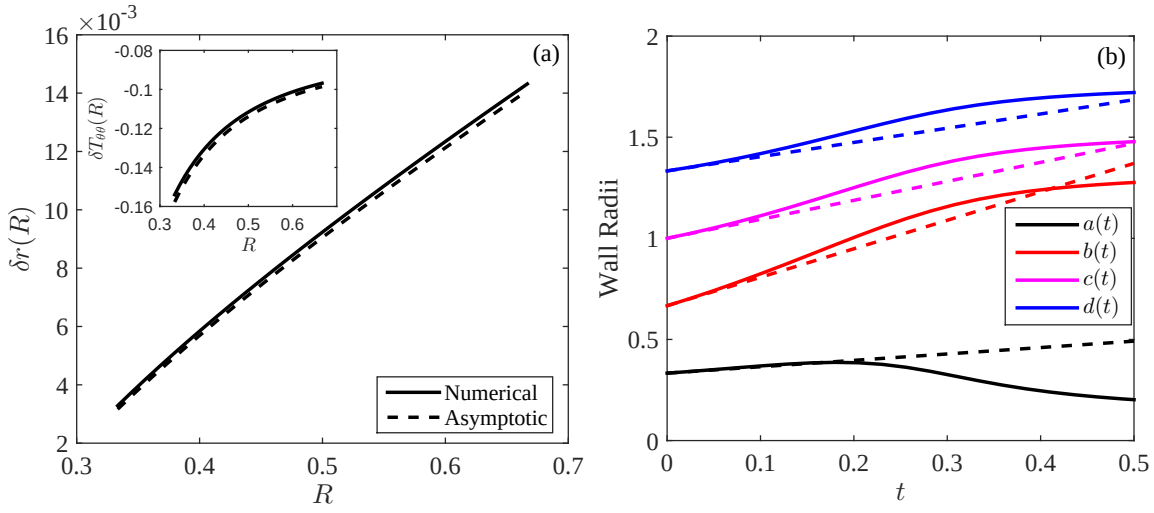

FIG. 3. Comparison of full numerical solution (solid lines) and asymptotic solution (4.1) (dashed lines). The perturbations δr and $\delta T_{\theta\theta}$ are shown as functions of reference frame coordinate R in the intima $A < R < B$ at time $t = 0.01$. Problem parameters are $P = 0$, $A = 1/3$, $B = 2/3$, $C = 1$, $D = 4/3$, $\mu_1 = 3$ kPa, $\mu_2 = 1.5$ kPa, $\mu_3 = 0.15$ kPa, $\eta_2 = 2.36$ kPa, $\eta_3 = 0.56$ kPa, $\beta_2 = 0.83$, $\beta_3 = 0.71$, $\varphi_2 = 29\pi/180$, $\varphi_3 = 62\pi/180$, $\nu_1 = 0.1$, $\nu_2 = 5$, $\lambda = 0$.

We now briefly study two simple cases: a pure elastic response ($\nu_1 > 0, \nu_2 = 0$) and cytokine-driven growth ($\nu_1 = 0, \nu_2 > 0$). These cases are helpful for understanding the general case of cytokine and stress-driven growth ($\nu_1 > 0, \nu_2 > 0$).

5.1 *Pure elastic response ($\nu_1 > 0$, $\nu_2 = 0$)*

When $\nu_2 = 0$, the growth rate is given by $\Gamma\tau = \nu_1(T_{\theta\theta} - \bar{T}_{\theta\theta}(r))$. Recall that the homeostatic stress, $\bar{T}_{\theta\theta}(r)$ is the stress distribution for a pressurized vessel when there is no PDGF so $T_{\theta\theta} = \bar{T}_{\theta\theta}(r)$. Therefore the growth rate is exactly zero with no cytokines and the vessel is in mechanical equilibrium. Thus we investigate how the deformation of the vessel wall changes with lumen pressure.

Measurements of intima-media thickness (IMT) are sometimes performed by clinicians to ascertain risk of cerebrovascular and cardiovascular events (Bots et al., 1997). For example, the carotid artery's IMT can be measured non-invasively using ultrasound (Aminbakhsh and Mancini, 1999). Figure 4 shows the initial deformation of the vessel wall along with the IMT. Recall that for $t < 0$, no internal pressure is applied but for $t > 0$, the lumen experiences a pressure P. The mean stress in the intima,

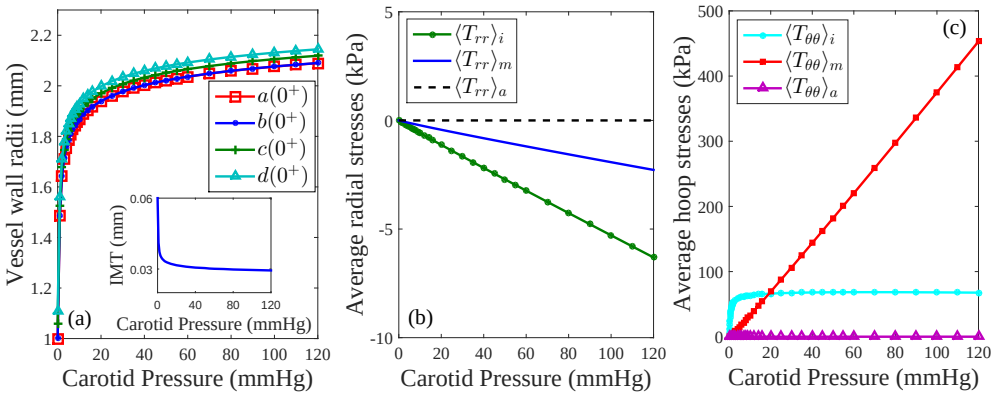

FIG. 4. (a) Initial response of vessel wall radii as a function of luminal pressure at $t = 0^+$. No growth is considered. Inset: IMT as a function of carotid pressure. (b) Mean stresses in the intima, media and adventitia associated with the initial response in (a). Model parameters are given in Table 1 with $\mu_1 = 100$ kPa.

media and adventitia are calculated as:

$$\langle T_{\theta\theta}\rangle_i = \frac{2}{b^2-a^2}\int_a^b T_{\theta\theta}(r)r\mathrm{d}r, \tag{5.1}$$

$$\langle T_{\theta\theta}\rangle_m = \frac{2}{c^2-b^2}\int_b^c T_{\theta\theta}(r)r\mathrm{d}r, \tag{5.2}$$

$$\langle T_{\theta\theta}\rangle_a = \frac{2}{d^2-c^2}\int_c^d T_{\theta\theta}(r)r\mathrm{d}r, \tag{5.3}$$

with the definitions for $\langle T_{rr}\rangle_i$, $\langle T_{rr}\rangle_m$ and $\langle T_{rr}\rangle_a$ identical to (5.1)-(5.3) but with $T_{\theta\theta}(r)$ replaced with $T_{rr}(r)$.

Our results in Figure 4(a) suggest that when the media deforms outwards, through conservation of mass, it must also thin. Therefore, IMT measurements can be (artificially) lowered. Generally, we see that when the pressure increases, the thicknesses of the intima and media both decrease, resulting in a smaller IMT.

Figures 4(b) and(c) shows that when the vessel is subjected to an internal pressure, the wall develops compressive radial stresses and tensile circumferential stresses. Stresses are relatively high in the intima and media compared with those in the adventitia. Another interesting observation is that at higher pressure, the tensile hoop stress in the media is larger than that of the intima. This is due to the proposed material properties of each layer. The media is assumed to be composed of an anisotropic model due to the presence of collagen fibers. As the applied pressure increases, the collagen fibers stiffen and become load-bearing. This limits arterial distension, as observed in Figure 4(a).

5.2 *Cytokine-driven growth ($\nu_1 = 0$, $\nu_2 > 0$)*

In this case, there is no "preferred" stress distribution for the vessel and the growth rate is $\Gamma\tau = \nu_2 u$. The time-evolution of the wall radii, stresses, the growth function, and other metrics are shown in Fig. 5. There is no homeostasis to inhibit tissue growth and therefore the growth function and hoop stress

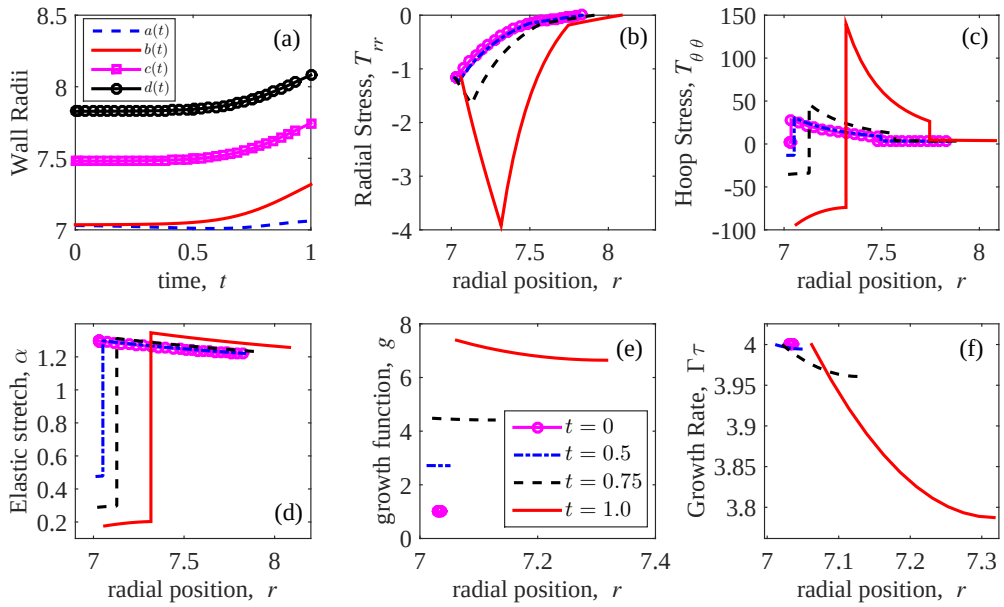

FIG. 5. Cytokine-driven growth for a rodent artery with $(\nu_1, \nu_2, \lambda) = (0, 4, 1.3)$. Other parameter values are from Table 2.

can increase without bound. As the intima rapidly expands, the resulting hoop stresses are orders of magnitude larger than radial stresses.

When $\nu_1 = 0$, it is generally more difficult to obtain convergence in the Newton iteration, and this is especially true for large values of ν_2. Taking a small positive value for ν_1 (which we do in the next section) appears to have a regularizing effect on the convergence.

5.3 *Cytokine and Stress-Driven Growth ($\nu_1 > 0$, $\nu_2 > 0$)*

With $\nu_1 > 0$, the homeostatic feedback in our model implies that intimal thickening is essentially stable. Given enough time, IMT should eventually saturate and the system finds a steady state corresponding to $\Gamma = 0$. In other words, the system evolves so that the hoop stress $T_{\theta\theta}$ satisfies

$$T_{\theta\theta}(r) = \bar{T}_{\theta\theta}(r) - \frac{\nu_2}{\nu_1}\left[\frac{K_1(\lambda b)I_0(\lambda r) + I_1(\lambda b)K_0(\lambda r)}{I_1(\lambda b)K_0(\lambda a) + I_0(\lambda a)K_1(\lambda b)}\right]. \tag{5.4}$$

We may interpret the right hand side of (5.4) as an effective homeostatic stress – it is the "baseline" homeostatic stress $\bar{T}_{\theta\theta}(r)$, modulated by the presence of growth factor with dimensionless decay rate λ. In steady state, g in eq. (2.26) must be independent of time. Therefore the growth rate, Γ must scale like $1/\hat{t}$, decreasing algebraically slowly. We were able to confirm this result numerically (results not shown). Given enough time, the hoop stress distribution reaches the effective homeostatic value, given by eq. (5.4) and intimal growth should saturate. This behavior is confirmed by data from animal experiments in the next section.

5.3.1 *Comparison with animal data*

The results of our model can be fit to data from animal models of atherosclerosis; specifically arterial denudation experiments on the iliac arteries of New Zealand White rabbits (Stadius et al., 1992) and the carotid arteries of Sprague-Dawley rats (Clowes et al., 1983). The experimental protocols in both studies were similar. The animals were anesthetized, the relevant artery was exposed through a wound and endothelial denudation was performed using a balloon catheter. Then the artery was ligated, the wound was closed and the animals were allowed to recover. In the rabbit experiments of Stadius et al. (1992) the animals were also put on a 2% cholesterol diet. Regularly throughout the course of the experiment, animals were sacrificed and morphometric measurements of the intima and media were made. In both sets of experiments, there was generally little change in the media area compared to the intima. In the rat experiments, each data point was an average over three animals. In the rabbit experiments, each data point came from a single animal.

A natural question to ask is if our model can reproduce the results from these experiments. In Figs. 6 and 8, we determine the parameters that best-fit our model using the Matlab optimization routine `fmincon.m` and estimate credible intervals for these parameters using a Bayesian approach and the Metropolis-Hastings algorithm.

We introduce random variables $\Theta = (\Theta_1, \Theta_2, \Theta_3) \equiv (-\log(\nu_1), \nu_2, -\log(\lambda))$ and Ω for the parameters and data, respectively. Let $\theta \equiv (\theta_1, \theta_2, \theta_3)$ and ω be particular realizations of Θ and Ω respectively. We denote the prior distribution of $(\Theta_1, \Theta_2, \Theta_3)$ as $P(\theta)$. Then Bayes' rule updates $P(\theta)$ in light of experimental data ω:

$$P(\theta|\omega) \propto P(\omega|\theta)P(\theta) \tag{5.5}$$

In eq. (5.5), the data ω consists of N pairs (t_i, Y_i), $i = 1, \ldots, N$, representing times at which animals were sacrificed and the corresponding measured intima area at that time. The likelihood function $P(\omega|\theta)$ is assumed to take the form

$$P(\omega|\theta) = \exp(-\chi^2), \tag{5.6}$$

$$\chi^2 = -\frac{1}{2}\sum_{i=1}^{N}\left[\frac{Y_i - y(t_i|\theta)}{\Delta}\right]^2, \tag{5.7}$$

where $y(t|\theta) \equiv \pi[b^2(t;\nu_1,\nu_2,\lambda) - a^2(t;\nu_1,\nu_2,\lambda)]$ is the intima area as predicted by our model and Δ is the approximate magnitude of error in the experiments (e.g. it could be the approximate length of the error bars). Note that the likelihood (5.6) is maximimized when the least-squares error $\chi^2 = \frac{1}{2\Delta^2}\sum_{i=1}^{N}[Y_i - y(t_i|\theta)]^2$ is minimized. For the prior $P(\theta)$, we take $P(\theta) = P_{\Theta_1}(\theta_1)P_{\Theta_2}(\theta_2)P_{\Theta_3}(\theta_3)$ where P_{Θ_1}, P_{Θ_2} and P_{Θ_3} are uniform densities with supports $[\ell_1, \ell_2]$, $[\ell_3, \ell_4]$ and $[\ell_5, \ell_6]$ respectively.

We use the Metropolis-Hastings algorithm to sample from the posterior density (5.5): see Appendix C. The algorithm is initialized with $(\theta_1^{(0)}, \theta_2^{(0)}, \theta_3^{(0)})$ which is found by (deterministically) minimizing χ^2 in the domain $[\ell_1, \ell_2] \times [\ell_3, \ell_4] \times [\ell_5, \ell_6]$ using Matlab's `fmincon.m` routine. The maximum likelihood estimates (MLE) and 95% credible intervals of Θ_1, Θ_2 and Θ_3 are given by the modes and [2.5,97.5] percentiles of the distributions P_{Θ_1}, P_{Θ_2} and P_{Θ_3}. Therefore, credible intervals for the best-fit parameters (ν_1, ν_2, λ) are in the form $[\exp(-\Theta_1^{(97.5)}), \exp(-\Theta_1^{(2.5)})]$ for ν_1, $[\Theta_2^{(2.5)}), \Theta_2^{(97.5)})]$ for ν_2 and $[\exp(-\Theta_3^{(97.5)}), \exp(-\Theta_3^{(2.5)})]$ for λ, where $X^{(p)}$ is the pth percentile for the random variable X. Increasing ν_1 in our model causes the intima area to saturate more quickly, increasing ν_2

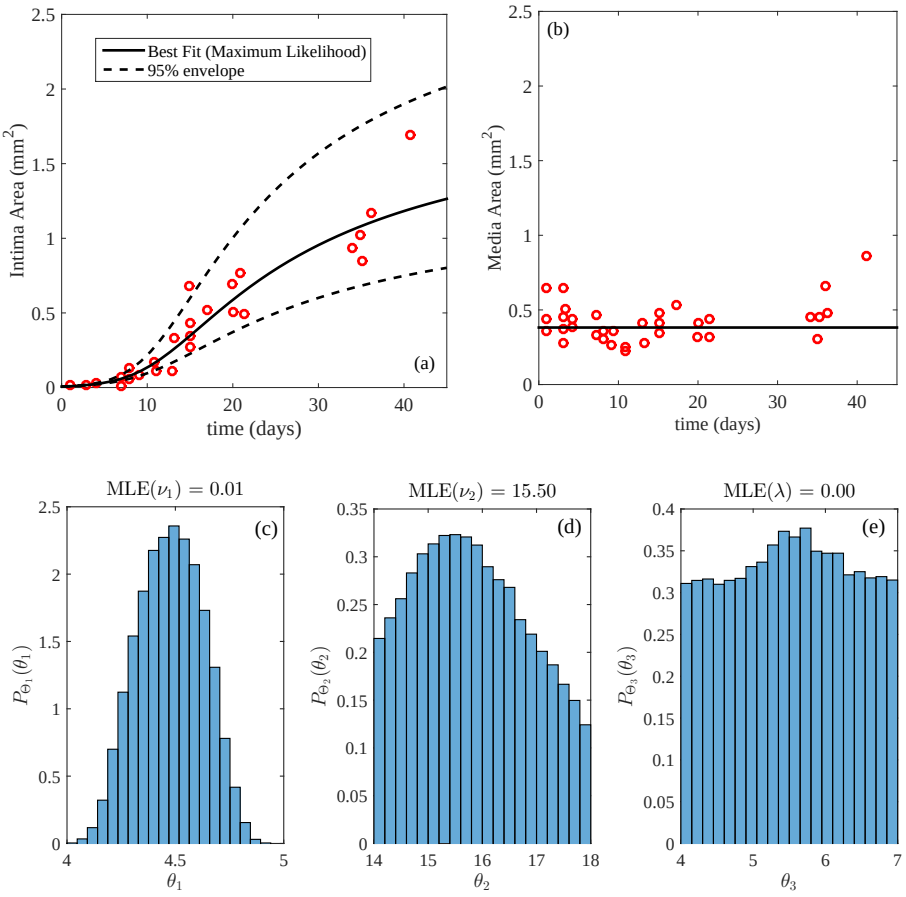

FIG. 6. (a,b) Intima and media areas of New Zealand white rabbits taken from Stadius et al. (1992) along with model prediction using best-fit parameters $(\nu_1, \nu_2, \lambda) = (0.01, 15.5, 0.00)$ and credible intervals obtained using the Metropolis-Hastings (MH) algorithm. Intima stiffness is $\mu_1 = 20$ kPa and all other parameters are taken from Table 1. (c,d,e) Marginal distributions of P_{Θ_1}, P_{Θ_2} and P_{Θ_3} with 20-bin resolution are used to calculate maximum likelihood estimates and credible intervals. The 2.5 and 97.5 percentiles for Θ_1, Θ_2 and Θ_3 are $(4.2, 4.8)$, $(14.1, 17.8)$ and $(4.1, 6.9)$ respectively. The dashed error-envelope in (a) corresponds to intima area development when $(\nu_1, \nu_2, \lambda) = (0.015, 14.1, 0.017)$ for the lower bound and $(0.01, 17.8, 0.00)$ for the upper bound. The MH parameters are numtrials = 180,000 samples, initial guess $\theta^{(0)} = [4.5099, 15.4323, 5.3391]$, $(\ell_1, \ell_2) = (4, 6)$, $(\ell_3, \ell_4) = (14, 18)$ and $(\ell_5, \ell_6) = (4, 7)$. Random walk stepsizes are $(\sigma_1, \sigma_2, \sigma_3) = (0.1, 0.2, 0.15)$ and the experimental error is estimated from the error bars in Stadius et al. (1992) as $\Delta = 0.2$ mm^2.

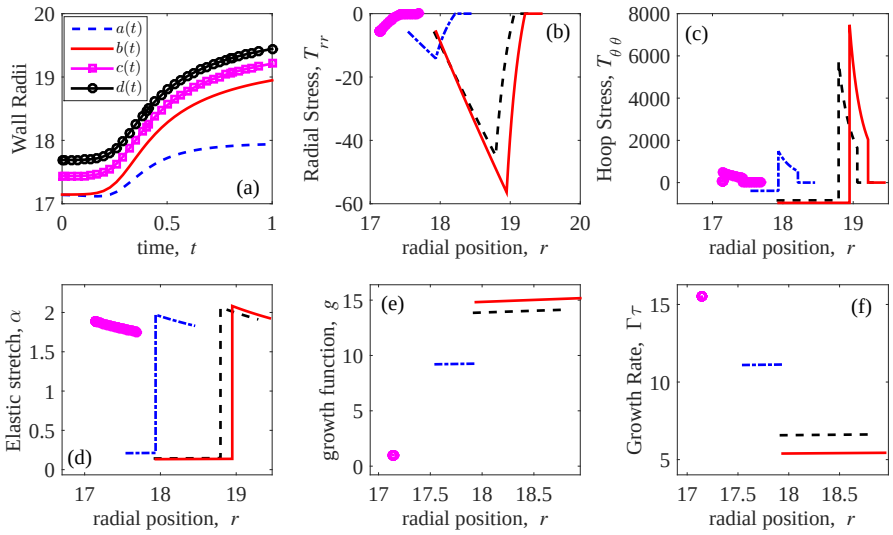

FIG. 7. Growth of a rabbit artery with parameters $(\nu_1, \nu_2, \lambda) = (0.01, 15.5, 0.00)$ corresponding to the best fit (thick solid) curve in Figure 6(a). (a) Wall boundaries $a(t)$, $b(t)$, $c(t)$ and $d(t)$ as functions of time t. Final time $t = 1$ corresponds to $\hat{t} = 45$ days. Note the rapid expansion of intima thickness $b - a$. (b)-(f) Radial stress, hoop stress, elastic stretch, growth function and dimensionless growth rate (see eq. (3.17)) are indicated at $t = 0, 0.4, 0.8$ and 1.0.

increases the rate of intima growth and increasing λ decreases the rate of change. Therefore, we construct an envelope of solutions, indicated by the dashed lines in Figs. 6(a) and 8(a) by solving our model with $(\nu_1, \nu_2, \lambda) = \left(\exp(-\Theta_1^{(97.5)}), \Theta_2^{(97.5)}, \exp(-\Theta_3^{(97.5)})\right)$ as the upper bound and $(\nu_1, \nu_2, \lambda) = \left(\exp(-\Theta_1^{(2.5)}), \Theta_2^{(2.5)}, \exp(-\Theta_3^{(2.5)})\right)$ as the lower bound. The solid lines represent the solutions using the MLEs of (ν_1, ν_2, λ). Our model assumes the media does not grow, so the media area is constant in time, as seen in Figs. 6(b) and 8(b).

Our numerical investigations suggest that determining the best-fit triple (ν_1, ν_2, λ) is a fairly ill-conditioned problem. Although the inference of Θ_1 seems to be well-conditioned, large changes in Θ_2 and Θ_3 only cause small changes in χ^2. We found that when the supports of our prior distributions were too large, the Metropolis-Hastings algorithm converged extremely slowly. Therefore, using the results of `fmincon.m` as a guide, we had to constrain the admissible values of θ_i (sometimes severely) in order to produce smooth distributions within a reasonable amount of time: see Figs. 6(c-e) and Figs. 8(c-e).

The MLEs for ν_1 and ν_2 for both the rabbit and rodent data satisfy $\nu_2 \gg \nu_1$, suggesting that growth of the intima is primarily driven by PDGF rather than a response to deviations from a homeostatic stress. Also, ν_1 and ν_2 change drastically between the two data sets. This is not too surprising because in addition to these parameters being organism-dependent, both ν_1 and ν_2 scale with τ (the total duration of the experiment) through eq. (3.18); and the rat experiments in Clowes et al. (1983) took roughly twice as long as the rabbit experiments in Stadius et al. (1992).

We find that the best-fit values of ν_1 and ν_2 are very sensitive to the initial intima thickness. The intimas of rats and rabbits do not normally contain any smooth muscle cells, unlike their human counter-

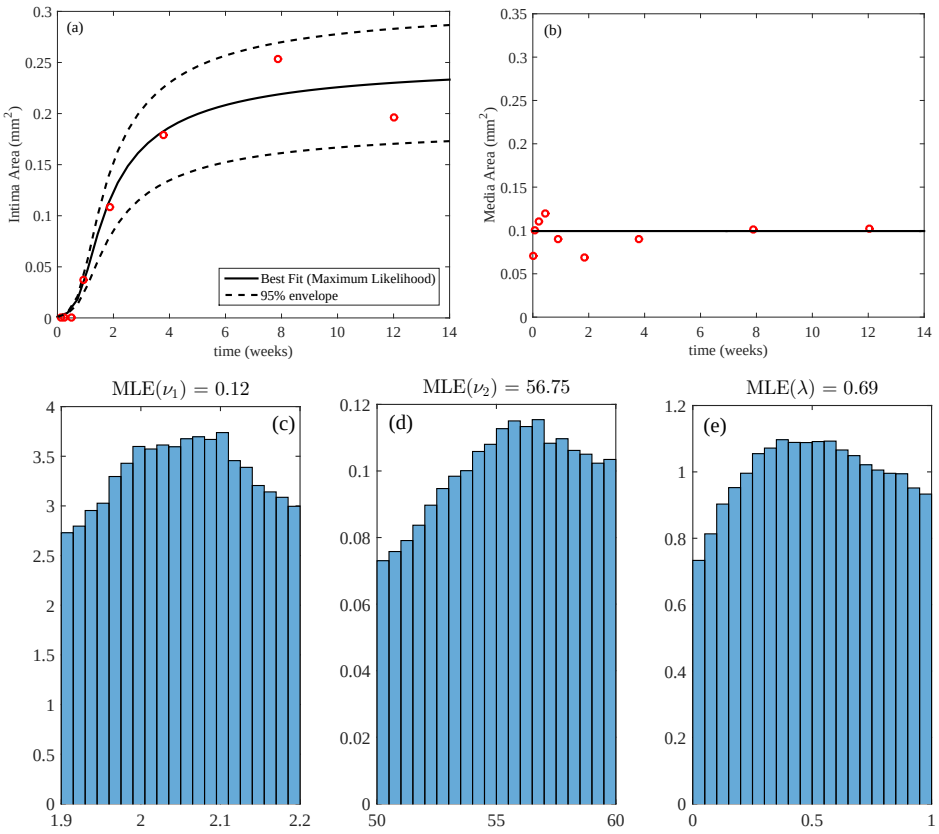

FIG. 8. (a,b) Intima and media areas of Sprague-Dawley rats taken from Clowes et al. (1983) along with model prediction using best-fit parameters $(\nu_1,\nu_2,\lambda) = (0.12, 56.8, 0.69)$ and credible intervals found using the Metropolis-Hastings (MH) algorithm. Intima stiffness is $\mu_1 = 20$ kPa and all other parameters are taken from Table 2. (c,d,e) Marginal distributions P_{Θ_1}, P_{Θ_2} and P_{Θ_3} with 20-bin resolution are used to calculate maximum likelihood estimates and credible intervals. The 2.5 and 97.5 percentiles for Θ_1, Θ_2 and Θ_3 are $(1.91, 2.19)$, $(50.3, 59.8)$ and $(0.03, 0.97)$ respectively. The dashed error-envelope in (a) corresponds to intima area development when $(\nu_1,\nu_2,\lambda) = (0.15, 50.8, 0.96)$ for the lower bound and $(0.11, 59.7, 0.39)$ for the upper bound. The MH parameters are numtrials = 223,000 samples, initial guess $\theta^{(0)} = [2.0326, 56.6247, 0.5273]$, $(\ell_1,\ell_2) = (1.9, 2.2)$, $(\ell_3,\ell_4) = (50, 60)$ and $(\ell_5,\ell_6) = (0, 1)$. Random walk stepsizes are $(\sigma_1,\sigma_2,\sigma_3) = (0.015, 0.5, 0.05)$, and the experimental error is estimated from the error bars in Clowes et al. (1983) as $\Delta = 0.05$ mm^2.

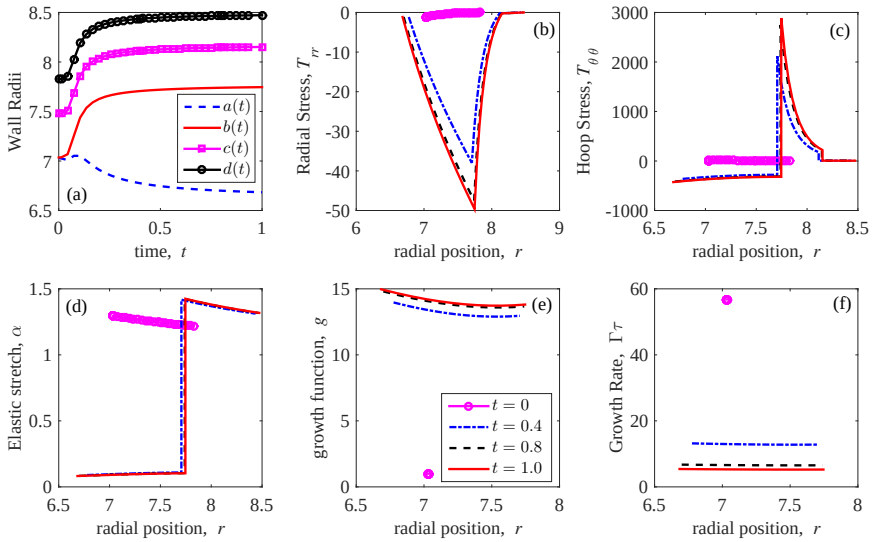

FIG. 9. Growth of a rodent artery with parameters $(\nu_1, \nu_2, \lambda) = (0.12, 56.8, 0.69)$ corresponding to the best fit (thick solid) curve in Figure 8(a). (a) Wall boundaries $a(t)$, $b(t)$, $c(t)$ and $d(t)$ as functions of time t. Final time $t = 1$ corresponds to $\hat{t}$ = 14 weeks. Note the rapid expansion of intima thickness $b - a$. (b)-(f) Radial stress, hoop stress, elastic stretch, growth function and dimensionless growth rate (see eq. (3.17)) are indicated at $t = 0, 0.4, 0.8$ and 1.0.

parts (Newby and Zaltsman, 1999): their intimas essentially consist of a single layer of endothelial cells, with $\hat{B} - \hat{A}$ smaller than any other lengthscale in our model. Ideally, we would like to take $\hat{B} - \hat{A} \to 0$. However, our model must be initialized with $B - A > 0$ because $B - A = 0 \Rightarrow b(t) - a(t) = 0$ for $t > 0$. The growth law (2.26) assumes that a material element in the intima grows exponentially in the absence of geometric constraints. It is therefore not surprising that the best-fit values for ν_1 and ν_2 are extremely sensitive to $B - A$. One way to "regularize" the model is to include the effect of cell-migration from the media (Fok, 2012) at early times, which would allow positive intima thickness for $t > 0$ even when $B - A = 0$. Interestingly, the experiments in Clowes et al. (1983) suggest that smooth muscle cell migration and proliferation are dominant in the early stages of the experiment while connective tissue synthesis is dominant in the later stages.

Figures 7 and 9 show wall evolutions, stress profiles, elastic stretches and growth-related functions for the best-fit parameters determined in Figs. 6 and 8. In both sets of experiments, there is a rapid buildup of hoop stress in the interface between the intima and media. We also see that the intimal expansion in the rabbit and rat experiments are qualitatively different. In the rabbit experiments, all 3 vessel wall layers dilate over time and there is a gradual increase in lumen area over the course of the experiment. On the other hand, in the rat experiments, our prediction is that the outer two layers quickly find their steady states and the lumen area *decreases* over time. For a given parameter set, whether $a(t)$ increases or decreases in time is an interesting (and open) question. The monotonicity of $a(t)$ is closely related to the important phenomenon of *Glagov remodeling* which we discuss in the next section.

The experimental measurements in Clowes et al. (1983) and Stadius et al. (1992) consist of intima *areas* of blood vessels extracted from animals sacrificed at different times. One could also quantify

intima growth by measuring the mean intima radius, (e.g. in an elliptic cross section, take the average of the semi-major and semi-minor axes). However, we strongly advocate the area method for two reasons. First, the extracted arterial cross sections are not exactly circular, so characterizing the growth by a radius is artificial and unnecessary. Second, when arteries are extracted and depressurized, their mean radii decrease: the radii for the lumen and internal/external laminas in a live animal are larger than those in the extracted cross sections. On the other hand, because the intima is largely incompressible, its area is independent of P, so *ex-vivo* measurements of the area should be identical to the *in-vivo* ones. From the modeling perspective, this is convenient since we do not have to mathematically "unload" our vessel cross section in order to compare with predictions from *ex-vivo* data.

5.3.2 *Glagov Remodeling* As noted in Section 2.2.3, the material properties of the intima can vary greatly. Here, we explore the effect of varying the intima stiffness μ_1, keeping all other parameters fixed: see Fig. 10. We find that the relative stiffness of the intima to the other layers determines whether the intima initially grows inward or outward. When μ_1 is small, $a(t)$ initially decreases because the outer layers are stiffer. On the other hand, when μ_1 is large, $a(t)$ initially increases because the media and adventitia are compliant relative to the intima. For large strains, the presence of collagen fibers in the media and adventitia ensure that these layers cannot dilate indefinitely.

When vessels undergo remodeling because of the presence of atherosclerotic plaque, they experience first an outward remodeling followed by inward remodeling. That is, vessel changes consist of two phases: first an outward expansion of the vessel wall accompanied by a slight *increase* in lumen area, followed by rapid constriction characterized by a *decrease* in lumen area. The second phase starts after the plaque burden exceeds about 40%. These changes in the vessel were first observed by Glagov et al. (1987) and are known as Glagov remodeling. Glagov quantified vessel remodeling by studying the lumen area L and the stenosis s of human coronary arteries:

$$L(t) = \pi a^2(t), \tag{5.8}$$

$$s(t) = 1 - \frac{a^2(t)}{b^2(t)} = \frac{\text{internal elastic lamina area} - \text{lumen area}}{\text{internal elastic lamina area}}. \tag{5.9}$$

As an artery remodels and becomes more diseased, both L and s change. Glagov remodeling is characterized by a curve $L(s)$ that is increasing for small s and decreasing for larger values of s. Stated mathematically, Glagov phenomenon occurs if there is a $s^* \in (0,1)$ such that $L'(s^*) = 0$ and $L''(s^*) < 0$. For human coronary arteries compromised by atherosclerosis, it appears that $s^* \approx 0.4$. We find that as intima stiffness increases in our model, a local maximum in $L(s)$ emerges for sufficiently large μ_1: see the insets in Fig. 10. Generally we find that s^* is sensitive to the reference radii $\hat{A}$, $\hat{B}$, $\hat{C}$ and $\hat{D}$ and insensitive to wall material properties. Interestingly, we also find that for long enough times, stenosis can decrease over time. Specifically, after about 5 years, $a(t)$ increases while $b(t)$, $c(t)$ and $d(t)$ remain approximately constant. We defer an analysis of this nonlinear phenomenon and a more detailed understanding of Glagov remodeling to a later publication.

5.3.3 *Effect of cytokine on IMT* The concentration of PDGF throughout the intima is controlled by the dimensionless decay rate, λ, and the growth constant, ν_2. In the non-dimensionalized model $\lambda = \sqrt{kL^2/D_c}$, where D_c is the PDGF diffusivity, k is the PDGF degradation rate and L is the initial IMT. If $\lambda \gg 1$, then the degradation rate is large compared to the diffusion rate, and PDGF is at a high concentration only near the lumen. Therefore, growth is also localized near the lumen. If $\lambda \ll 1$, then

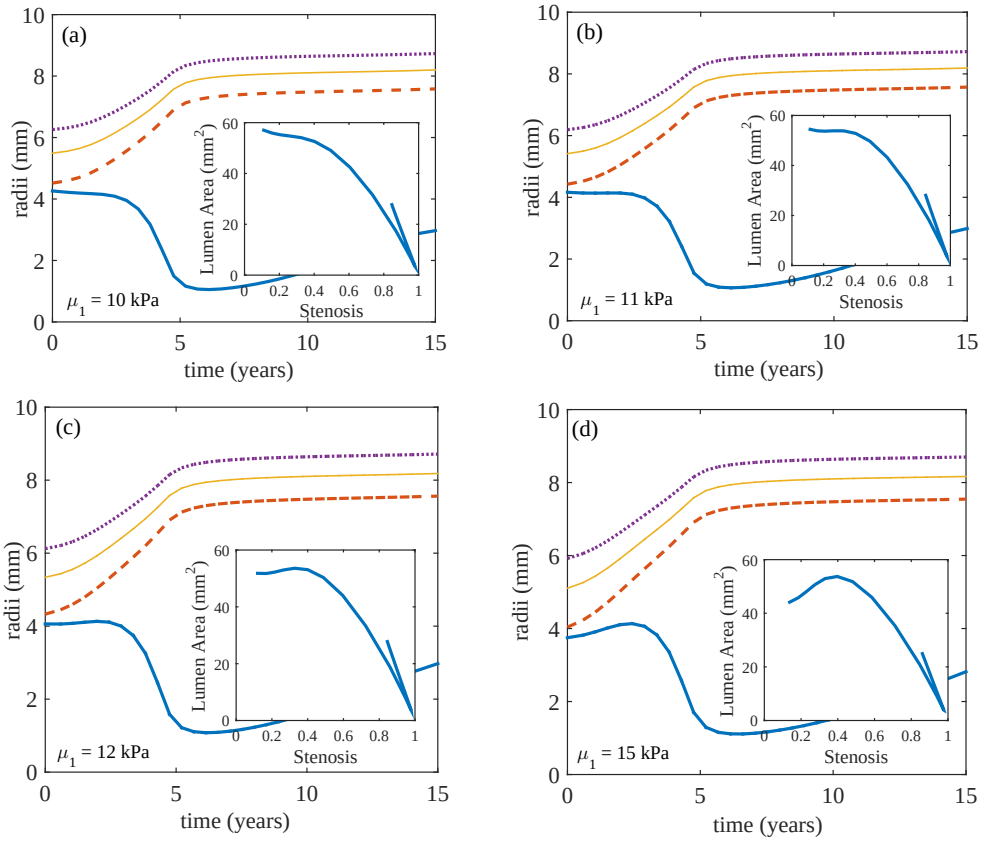

FIG. 10. Increase in intima thickness of an artery after injury to the endothelium for different intima stiffnesses μ_1. Glagov remodeling emerges for sufficiently large μ_1. (a) $\mu_1 = 10$ kPa, (b) $\mu_1 = 11$ kPa, (c) $\mu_1 = 12$ kPa, (d) $\mu_1 = 15$ kPa. Common parameters are $(\nu_1, \nu_2, \lambda) = (0.01, 30, 0.01)$, $\tau = 15$ years, $\mu_2 = 8$ kPa, $\eta_2 = 4$ kPa, $\beta_2 = 0.83$, $\varphi_2 = 50\pi/180$, $\mu_3 = 0.2$ kPa, $\eta_3 = 4$ kPa, $\beta_3 = 0.71$, $\varphi_3 = 62\pi/180$, $P = 100$ mmHg, $\hat{A} = 2$ mm, $\hat{B} = 2.5$ mm, $\hat{C} = 4$ mm, $\hat{D} = 5$ mm. Wall radii $a(t)$, $b(t)$, $c(t)$ and $d(t)$ are represented by thick solid, dashed, thin solid and dotted lines respectively.

the degradation rate is small compared to the diffusion rate, and PDGF is present at high concentrations throughout the entire intima and the entire intima grows. We point out that the decay length of PDGF λ^{-1} must be large compared to the intima thickness $b(t)-a(t)$ for the entire intima to grow (equivalently: $\sqrt{D_c/k} \gg \hat{b}-\hat{a}$). This is a dynamic condition which may be violated for later times. Even though $\lambda \ll 1$, the intima can grow thick enough so that there is significant spatial decay in the cytokine. Different layers of the intima will then experience different growth rates. The evolution of IMT for different λ is shown in Fig. 11(a). For small λ, all tissue in the intima has access to high levels of PDGF and the tissue initially grows rapidly. For large λ, the PDGF is degraded at a high rate and the diffusion constant is small which results in limited growth. This plot confirms our belief that in order for substantial IMT growth to occur (as seen in Figs. 6 and 8), we require $\lambda \ll 1$.

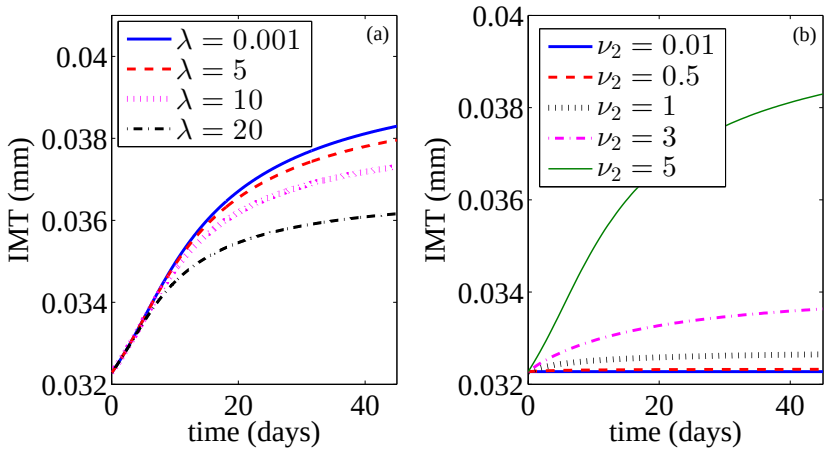

FIG. 11. (a) IMT evolution for different λ. Parameters are $\nu_1 = 0.018$, $\nu_2 = 20$, $\mu_1 = 20$ kPa and other parameter values are taken from Table 1. (b) IMT evolution for different ν_2. Parameters are $\nu_1 = 0.018$, $\lambda = 0.348$ and $\mu_1 = 20$ kPa. Other parameter values are taken from Table 1.

The dimensionless parameter, ν_2, is a measure of how much the growth is modified by the presence of cytokine. A larger value of ν_2 means that the growth rate is larger for a given concentration of PDGF. The general effect of increasing ν_2 is to induce the intima to grow more rapidly. For all $\nu_2 \geqslant 0$, the IMT eventually saturates, but increasing ν_2 increases the saturating level. See Fig. 11(b).

6. Conclusions

In this paper we presented a model for intimal hyperplasia that typically occurs after angioplasty in humans or in animal models of atherosclerosis. The model makes predictions for the evolution of intima, media and adventitia thicknesses. Related quantities such as the important intima-media thickness (IMT) can be quickly inferred. Our model is based on the theory of hyperelastic materials and predicts the stress distribution within concentric lesions. The distribution of cytokines within the intima can result in uniform or differential growth. The result is a rich set of dynamic behaviors e.g. remodeling that switches from inward-to-outward or outward-to-inward, IMT growth that depends on cytokine half-life and material properties of the vessel wall; and unintuitive results such as decreasing IMT and stenosis

under positive growth. Importantly, our mathematical model is the first that we know of that exhibits the phenomenon of Glagov remodeling, where the lumen expands, or remains roughly constant, before constricting as the intima thickens.

Our model predicts that for the intima growth shown in Figs. 6 and 8, growth must occur uniformly throughout the intima. Intramural flow may also be responsible for enhanced transport and distribution of PDGF giving rise to uniform cytokine distributions. If our description of the layer properties of the vessel are correct and the intima and media are hyperelastic, our model predicts that homeostatic control of the growth is very weak ($\nu_1 \ll \nu_2$): if there is a "preferred" distribution of stress in the artery, the local growth is not strongly affected by it. Instead, our results suggest that intimal growth is driven primarily by cytokines which persistently increase the stresses in the intima and media.

In our model we assume zero traction on the outer boundary. In human carotid arteries there is likely a reactive radial stress on the outer boundary due to the perivascular tissue pushing back on the vessel as the tissue grows outward. The form of the outermost boundary condition is still unclear at present and there has yet to be any agreement on the best way to model this aspect of the *in-vivo* mechanics. Humphrey and Na (2002) proposed a simple exponential form for the perivascular reactive radial stress but this form was not based on data. Preliminary results of including this exponential boundary condition in our model produced the same qualitative behavior as we observed when using a zero traction boundary condition.

While the medical focus of our model was on GVD in humans and atherosclerotic lesions in rabbits and rodents, we believe our framework could be applicable to other conditions too. For example, aneurysms and hypertension both involve substantial remodeling-in-time of blood vessels. Recent research on asthma by Ronzani et al. (2014) suggests that remodeling in the epithelial layer of the respiratory tract can also arise from inflammation. In this system, epithelial cells release cytokines such as thymic stromal lymphopoietin (TSLP) and granulocyte macrophage colony stimulating factor (GM-CSF), in much the same way that platelets release PDGF on the endothelial surface in our model. However, one should take precautions about using this model to describe human atherosclerosis. Advanced atherosclerotic lesions are eccentric and highly heterogeneous containing (for example) necrotic cores and extensive calcification. Such lesions would require a more general, non-axisymmetric model whose material properties can change temporally and spatially. The simple geometry assumed in our model means that our predictions are limited to lesions that are approximately concentric.

A natural extension to our current work is to use our model to understand Glagov remodeling in terms of competing stiffnesses of different vessel wall layers. The fact that the critical stenosis (beyond which lumen area rapidly decreases) is strongly dependent on vessel geometry but only weakly dependent on parameters in the strain energy function could be proved mathematically. Another extension is to follow Ben Amar et al. (2011) and perform linear stability analysis on the growing concentric lesion to see if it is stable. This calculation may help us understand why many atherosclerotic lesions are eccentric. Our model can also be extended by allowing the growth function to depend on several chemical species which could react with each other through mass-action or Michaelis-Menten kinetics. Many of the main biochemical pathways that lead to smooth muscle cell proliferation, for example, have already been established and it should be possible to include these reactions in our model to see what effect they have on intimal growth.

In short, we believe our model exhibits many interesting mathematical features and may be useful for describing several medical conditions that involve vessel remodeling. We hope that it will stimulate further quantitative study of such conditions.

Acknowledgments

This work was supported by a grant from the Simons Foundation (282579 to Pak-Wing Fok).

References

Ali C Akyildiz, Lambert Speelman, Harald van Brummelen, Miguel A Gutiérrez, Renu Virmani, Aad van der Lugt, AF Van Der Steen, Jolanda J Wentzel, and FJ Gijsen. Effects of intima stiffness and plaque morphology on peak cap stress. *Biomed Eng Online*, 10(1):1–13, 2011.

D Ambrosi and F Mollica. On the mechanics of a growing tumor. *International Journal of Engineering Science*, 40(12):1297–1316, 2002.

D Ambrosi and F Mollica. The role of stress in the growth of a multicell spheroid. *Journal of mathematical biology*, 48(5):477–499, 2004.

A. Aminbakhsh and G. B. J. Mancini. Carotid intima-media thickness measurements: what defines an abnormality? A systematic review. *Clinical and Investigative Medicine*, 22:149–157, 1999.

P. Badel, S. Avril, S. Lessner, and M. Sutton. Mechanical identification of hyperelastic anisotropic properties of mouse carotid arteries. In *Mechanics of Biological Systems and Materials, Volume 2*, pages 11–17. Springer, 2011.

Radj A Baldewsing, Chris L de Korte, Johannes A Schaar, Frits Mastik, and Antonius FW van der Steen. Finite element modeling and intravascular ultrasound elastography of vulnerable plaques: parameter variation. *Ultrasonics*, 42(1):723–729, 2004.

SRH Barrett, MPF Sutcliffe, S Howarth, Z-Y Li, and JH Gillard. Experimental measurement of the mechanical properties of carotid atherothrombotic plaque fibrous cap. *Journal of biomechanics*, 42 (11):1650–1655, 2009.

M. Ben Amar, A. Goriely, M. M. Muller, and L. Cugliandolo, editors. *New Trends in the Physics and Mechanics of Biological Systems: Lecture Notes of the Les Houches Summer School, Volume 92, July 2009*. Oxford University Press, 2011.

D. Bluestein, Y. Alemu, I. Avrahami, M. Gharib, K. Dumont, J. J. Ricotta, and S. Einav. Influence of microcalcifications on vulnerable plaque mechanics using fsi modeling. *Journal of Biomechanics*, 41:1111–1118, 2008.

Gustav VR Born and Peter D Richardson. Mechanical properties of human atherosclerotic lesions. In *Pathobiology of the human atherosclerotic plaque*, pages 413–423. Springer, 1990.

M. L. Bots, A. W. Hoes, P. J. Koudstaal, A. Hofman, and D. E. Grobbee. Common carotid intima-media thickness and risk of stroke and myocardial infarction. *Circulation*, 96:1432–1437, 1997.

A. H. Chau, R. C. Chan, M. Shishkov, B. MacNeil, N. Iftimia, G. J. Tearney, R. D. Kamm, B. E. Bouma, and M. R. Kaazempur-Mofrad. Mechanical analysis of atherosclerotic plaques based on optical coherence tomography. *Annals of Biomedical Engineering*, 32:1494 – 1503, 2004.

G. C. Cheng, H. M. Loree, R. D. Kamm, M. C. Fishbein, and R. T. Lee. Distribution of circumferential stress in ruptured and stable atherosclerotic lesions. a structural analysis with histopathological correleation. *Circulation*, 87:1179–1187, 1993.

Alexander W Clowes, Michael A Reidy, and MM Clowes. Mechanisms of stenosis after arterial injury. *Laboratory investigation; a journal of technical methods and pathology*, 49(2):208–215, 1983.

P.B. Dobrin and A.A. Rovick. Influence of vascular smooth muscle on contractile mechanics and elasticity of arteries. *American Journal of Physiology–Legacy Content*, 217(6):1644–1651, 1969.

P.-W. Fok. Growth of Necrotic Cores in Atherosclerotic Plaque. *Mathematical Medicine and Biology*, 2011.

P.-W. Fok. Mathematical model of intimal thickening in atherosclerosis: Vessel stenosis as a free boundary problem. *Journal of Theoretical Biology*, 314:23–33, 2012.

M. H. Friedman. A biologically plausible model of thickening of arterial intima under shear. *Arteriosclerosis, Thrombosis and Vascular Biology*, 9:511 – 522, 1989.

K Garikipati, EM Arruda, K Grosh, H Narayanan, and S Calve. A continuum treatment of growth in biological tissue: the coupling of mass transport and mechanics. *Journal of the Mechanics and Physics of Solids*, 52(7):1595–1625, 2004.

T Christian Gasser, Ray W Ogden, and Gerhard A Holzapfel. Hyperelastic modelling of arterial layers with distributed collagen fibre orientations. *Journal of the royal society interface*, 3(6):15–35, 2006.

S. Glagov, E. Weisenberg, C. K. Zarins, R. Stankunavicius, and G. J. Kolettis. Compensatory enlargement of human atherosclerotic coronary arteries. *New England Journal of Medicine*, 316:1371 – 1375, 1987.

A. Goriely and M. Ben Amar. On the definition and modeling of incremental, cumulative and continuous growth laws in morphoelasticity. *Biomechanics and Modeling in Mechanobiology*, 6(5):289–296, 2007.

H. Hanke, T. Strohschneider, M. Overhoff, E. Betz, and K. R. Karsch. Time course of smooth muscle cell proliferation in the intima and media of arteries following experimental angioplasty. *Circulation Research*, 67:651–659, 1990.

W. Hao and A. Friedman. The ldl-hdl profile determines the risk of atherosclerosis: A mathematical model. *PLoS ONE*, 9:e90497, 2014. doi: doi:10.1371/journal.pone.0090497.

R. Heuchel, A. Berg, M. Tallquist, K. Ahlen, R.K. Reed, K. Rubin, L. Claesson-Welsh, C.-H. Heldin, and P. Soriano. Platelet-derived growth factor β receptor regulates interstitial fluid homeostasis through phosphatidylinositol-3' kinase signaling. *Proceedings of the National Academy of Sciences*, 96:11410 –11415, 1999.

G. Holzapfel, G. Sommer, C. Gasser, and P. Regitnig. Determination of layer-specific mechanical properties of human coronary arteries with nonatherosclerotic intimal thickening and related constitutive modeling. *Am. J. Physiol. Heart. Circ. Physiol.*, 289:H2048 – H2058, 2005.

Gerhard A Holzapfel. Biomechanics of soft tissue. *The handbook of material behavior*, 2000.

H. Huang, R. Virmani, H. Younis, A. P. Burke, R. D. Kamm, and R. T. Lee. The impact of calcification on the biomechanical stability of atherosclerotic plaques. *Circulation*, 103:1051 – 1056, 2001.

JD Humphrey and S Na. Elastodynamics and arterial wall stress. *Annals of biomedical engineering*, 30 (4):509–523, 2002.

A. I. Ibragimov, C. J. McNeal, L. R. Ritter, and J. R. Walton. A mathematical model of atherogenesis as an inflammatory response. *Mathematical medicine and biology : a journal of the IMA*, 22(4):305–33, December 2005. ISSN 1477-8599. doi: 10.1093/imammb/dqi011. URL `http://www.ncbi.nlm.nih.gov/pubmed/16162594`.

C. L. Jackson, E. W. Raines, R. Ross, and M. A. Reidy. Role of endogenous platelet-derived growth factor in arterial smooth muscle cell migration after balloon catheter injury. *Arteriosclerosis, Thrombosis and Vascular Biology*, 13:1218–1226, 1993.

DN Kim, H Imai, J Schmee, KT Lee, and WA Thomas. Intimal cell mass-derived atherosclerotic lesions in the abdominal aorta of hyperlipidemic swine part 1. cell of origin, cell divisions and cell losses in first 90 days on diet. *Atherosclerosis*, 56(2):169–188, 1985.

R. W. Lawton. The thermoelastic behavior of isolated aortic strips of the dog. *Circulation research*, 2 (4):344–353, 1954.

R.T. Lee, S.G. Richardson, H.M. Loree, A.J. Grodzinsky, S.A. Gharib, F.J. Schoen, and N. Pandian. Prediction of mechanical properties of human atherosclerotic tissue by high-frequency intravascular ultrasound imaging. an in vitro study. *Arteriosclerosis, Thrombosis, and Vascular Biology*, 12(1):1–5, 1992.

VA Lubarda and A Hoger. On the mechanics of solids with a growing mass. *International journal of solids and structures*, 39(18):4627–4664, 2002.

Gangming Luo, Stephen C Cowin, Ali M Sadegh, and Yves P Arramon. Implementation of strain rate as a bone remodeling stimulus. *Journal of biomechanical engineering*, 117(3):329–338, 1995.

Ingrid Masson, Pierre Boutouyrie, Stéphane Laurent, Jay D Humphrey, and Mustapha Zidi. Characterization of arterial wall mechanical behavior and stresses from human clinical data. *Journal of biomechanics*, 41(12):2618–2627, 2008.

R. N. Mitchell. Graft vascular disease: Immune response meets the vessel wall. *Annu. Rev. Pathol. Mech. Dis.*, 4:19–47, 2009.

M. J. Mulvaney. Small artery remodeling in hypertension. *Current Hypertension Reports*, 4:49 – 55, 2002.

Andrew C Newby and Alla B Zaltsman. Fibrous cap formation or destructionthe critical importance of vascular smooth muscle cell proliferation, migration and matrix formation. *Cardiovascular research*, 41(2):345–360, 1999.

A. Ougrinovskaia, R. S. Thompson, and M. R. Myerscough. An ODE Model of Early Stages of Atherosclerosis: Mechanisms of the Inflammatory Response. *Bulletin of mathematical biology*, pages 1534–1561, May 2010. ISSN 1522-9602. doi: 10.1007/s11538-010-9509-4. URL `http://www.ncbi.nlm.nih.gov/pubmed/20440571`.

Gerard Pasterkamp, Peter JW Wensing, Mark J Post, Berend Hillen, Willem PTM Mali, and Cornelius Borst. Paradoxical arterial wall shrinkage may contribute to luminal narrowing of human atherosclerotic femoral arteries. *Circulation*, 91(5):1444–1449, 1995.

Sunita R. Patel, John H. Hartwig, and Joseph E. Italiano Jr. The biogenesis of platelets from megakaryocyte proplatelets. *The Journal of Clinical Investigation*, 115(12):3348–3354, 12 2005. doi: 10.1172/JCI26891.

E.K. Rodriguez, A. Hoger, and A.D. McCulloch. Stress-dependent finite growth in soft elastic tissues. *Journal of biomechanics*, 27(4):455–467, 1994.

C. Ronzani, A. Casset, and F. Pons. Exposure to multi-walled carbon nanotubes results in aggravation of airway inflammation and remodeling and in increased production of epithelium-derived innate cytokines in a mouse model of asthma. *Arch. Toxicol.*, 88:489 – 499, 2014.

M. L. Stadius, R. Rowan, J. F. Fleischhauer, R. Kernoff, M. Billingham, and A. M. Gown. Time course and cellular characteristics of the iliac artery response to acute balloon injury. an angiographic, morphometric, and immunocytochemical analysis in the cholesterol-fed new zealand white rabbit. *Arteriosclerosis, Thrombosis and Vascular Biology*, 12:1267–1273, 1992.

A. V. Sterpetti, A. Cucina, L. S. D'Angelo, B. Cardillo, and A. Cavallaro. Shear stress modulates the proliferation rate, protein synthesis, and mitogenic activity of arterial smooth muscle cells. *Surgery*, 113:691–699, 1993.

Larry A Taber. Biomechanics of growth, remodeling, and morphogenesis. *Applied mechanics reviews*, 48(8):487–545, 1995.

Larry A Taber and Jay D Humphrey. Stress-modulated growth, residual stress, and vascular heterogeneity. *Journal of biomechanical engineering*, 123(6):528–535, 2001.

H. Ueba, M. Kawakami, and T. Yaginuma. Shear stress as an inhibitor of vascular smooth muscle cell proliferation. *Arteriosclerosis, Thrombosis and Vascular Biology*, 17:1512–1516, 1997.

A. E. van der Wijk, M. P. Schreurs, and M. J. Cipolla. Pregnancy causes diminished myogenic tone and outward hypotrophic remodeling of the cerebral vein of galen. *J. Cereb. Blood Flow Metab.*, 33:542 – 549, 2013.

KY Volokh. Stresses in growing soft tissues. *Acta Biomaterialia*, 2(5):493–504, 2006.

Brian H Wayman, W Robert Taylor, Alexander Rachev, and Raymond P Vito. Arteries respond to independent control of circumferential and shear stress in organ culture. *Annals of biomedical engineering*, 36(5):673–684, 2008.

Y. Yu, M. Sweeney, S. Zhang, O. Platoshyn, J. Landsberg, A. Rothman, and J. X.-J. Yuan. PDGF stimulates pulmonary vascular smooth muscle cell proliferation by upregulating TRPC6 expression. *Americal Journal of Physiology – Cell Physiology*, 284:C316–X330, 2003.

A. Numerical Procedure

The primary quantities of interest are the time-evolution of the wall radii a, b, c and d and the stress distributions $T_{rr}(R)$ and $T_{\theta\theta}(R)$. Recall that all quantities depend on time t solely through the growth function $g(r,t)$. Because our model's dependence on t is purely algebraic (there are no t-derivatives in any of the equations), we often omit explicit dependence on t in the dependent variables when presenting the equations.

Here we describe our numerical method to compute these quantities at a a sequence of time points $t \in \{0 \equiv t_0 < t_1 < t_2 < \ldots < t_m\}$. The definitions of frequently used functions Q_1, Q_2 and Q_3 are given in eqs. (2.18)-(2.20).

1. Suppose $t = 0$. There is no growth ($g = 1$) and no release of cytokine. Deformation of the vessel wall arises only from the blood pressure. With a, b and c regarded as the unknowns, solve the nonlinear system of equations

$$\int_A^B \frac{Q_1[\alpha(R;a,b,c)]\mathrm{d}R}{R} + \int_B^C \frac{Q_2[\alpha(R;a,b,c)]\mathrm{d}R}{R} + \int_C^D \frac{Q_3[\alpha(R;a,b,c)]\mathrm{d}R}{R} = \frac{P}{\eta_2}, \quad \text{(A.1)}$$

$$r(B) = b, \quad \text{(A.2)}$$

$$r(C) = c, \quad \text{(A.3)}$$

where $r(R) = \left(a^2 + R^2 - A^2\right)^{1/2}$ and let

$$\alpha(R;a,b,c) = \begin{cases} \dfrac{\left(a^2+R^2-A^2\right)^{1/2}}{R}, & A \leqslant R \leqslant B, \\ \dfrac{\left(b^2+R^2-B^2\right)^{1/2}}{R}, & B < R \leqslant C, \\ \dfrac{\left(c^2+R^2-C^2\right)^{1/2}}{R}, & C < R \leqslant D. \end{cases} \quad \text{(A.4)}$$

This yields the wall positions $a(0)$, $b(0)$, $c(0)$. The outermost boundary $d(0)$ immmediately follows from $d(0) = r(D)$.

2. Let

$$T_{rr}(R) = \begin{cases} -\dfrac{P}{\eta_2} + \displaystyle\int_A^R Q_1[\alpha(R')]\frac{\mathrm{d}R'}{R'}, & A \leqslant R \leqslant B, \\ -\displaystyle\int_C^D Q_3[\alpha(R')]\frac{\mathrm{d}R'}{R'} - \int_R^C Q_2[\alpha(R')]\frac{\mathrm{d}R'}{R'}, & B < R \leqslant C, \\ -\displaystyle\int_R^D Q_3[\alpha(R')]\frac{\mathrm{d}R'}{R'}, & C < R \leqslant D, \end{cases} \quad \text{(A.5)}$$

$$T_{\theta\theta}(R) = \bar{T}_{\theta\theta}(R) \quad = \quad \begin{cases} \alpha^2(R)Q_1[\alpha(R)] + T_{rr}(R), & A \leqslant R \leqslant B, \\ \alpha^2(R)Q_2[\alpha(R)] + T_{rr}(R), & B < R \leqslant C, \\ \alpha^2(R)Q_3[\alpha(R)] + T_{rr}(R), & C < R \leqslant D. \end{cases} \tag{A.6}$$

3. For $i = 1, 2, \ldots, m$, find $T_{\theta\theta}(R,t_i)$, $r(R,t_i)$, $a(t_i)$, $b(t_i)$, $c(t_i)$, $d(t_i)$ that satisfy

$$M(T_{\theta\theta}, r, a, b, c, d, t_i) = \mathbf{0}, \tag{A.7}$$

using a Newton iteration. The function M is defined below. Use $T_{\theta\theta}(R,t_{i-1})$, $r(R,t_{i-1})$, $a(t_{i-1})$, $b(t_{i-1})$, $c(t_{i-1})$, $d(t_{i-1})$ as starting guesses to the iteration. In MATLAB, the Newton iteration can be implemented using `fsolve` and all integrals are discretized using a compound trapezium rule with $N = 12$ abscissae.

The function M is defined as

$$M = \begin{pmatrix} F_1(R) \\ F_2(R) \\ F_3 \\ F_4 \\ F_5 \\ F_6 \end{pmatrix} = \begin{pmatrix} T_{\theta\theta}^{(new)}(R) - T_{\theta\theta}(R) \\ r^{(new)}(R) - r(R) \\ \underbrace{\int_A^B \frac{Q_1[\alpha(R)]\mathrm{d}R}{R}}_{F_{31}} + \underbrace{\int_B^C \frac{Q_2[\alpha(R)]\mathrm{d}R}{R}}_{F_{32}} + \underbrace{\int_C^D \frac{Q_3[\alpha(R)]\mathrm{d}R}{R}}_{F_{33}} - \frac{P}{\eta_2}, \\ r^{(new)}(D) - d \\ r^{(new)}(C) - c \\ r^{(new)}(B) - b \end{pmatrix}, \tag{A.8}$$

where

$$r^{(new)}(R) = \begin{cases} \left(a^2 + 2\int_A^R g^2(R')R'\mathrm{d}R'\right)^{1/2}, & A \leqslant R \leqslant B, \\ \left(b^2 + R^2 - B^2\right)^{1/2}, & B < R \leqslant C, \\ \left(c^2 + R^2 - C^2\right)^{1/2}, & C < R \leqslant D. \end{cases} \tag{A.9}$$

$$g(R) = \exp\left[\frac{\nu_2 t}{2} \cdot \frac{K_1(\lambda b)I_0(\lambda r(R)) + I_1(\lambda b)K_0(\lambda r(R))}{I_1(\lambda b)K_0(\lambda a) + I_0(\lambda a)K_1(\lambda b)}\right] \times \exp\left[\frac{\nu_1\left(T_{\theta\theta}(R) - \bar{T}_{\theta\theta}(R)\right)t}{2}\right], \tag{A.10}$$

$$\alpha(R) = \begin{cases} \dfrac{r^{(new)}(R)}{Rg(R)}, & A \leqslant R \leqslant B, \\ \dfrac{r^{(new)}(R)}{R}, & B < R \leqslant D. \end{cases} \tag{A.11}$$

$$T_{rr}^{(new)}(R) = \begin{cases} -\dfrac{P}{\eta_2} + \displaystyle\int_A^R Q_1[\alpha(R')]\frac{\mathrm{d}R'}{R'}, & A \leqslant R \leqslant B, \\ -\displaystyle\int_C^D Q_3[\alpha(R')]\frac{\mathrm{d}R'}{R'} - \int_R^C Q_2[\alpha(R')]\frac{\mathrm{d}R'}{R'}, & B < R \leqslant C, \\ -\displaystyle\int_R^D Q_3[\alpha(R')]\frac{\mathrm{d}R'}{R'}, & C < R \leqslant D. \end{cases} \tag{A.12}$$

$$T_{\theta\theta}^{(new)}(R) = \begin{cases} \alpha^2(R)Q_1[\alpha(R)] + T_{rr}^{(new)}(R), & A \leqslant R \leqslant B, \\ \alpha^2(R)Q_2[\alpha(R)] + T_{rr}^{(new)}(R), & B < R \leqslant C, \\ \alpha^2(R)Q_3[\alpha(R)] + T_{rr}^{(new)}(R), & C < R \leqslant D, \end{cases} \tag{A.13}$$

Note that the function $M(T_{\theta\theta}, r, a, b, c, d, t)$ takes t, $T_{\theta\theta}(R,t)$, $r(R,t)$, $a(t)$, $b(t)$, $c(t)$, $d(t)$ as inputs and takes A, B, C, D, ν_1, ν_2, λ, P/η_2, μ_1/η_2, μ_2/η_2, μ_3/η_2, η_1/η_2, η_3/η_2 and $\bar{T}_{\theta\theta}(R)$ as parameters. While F_3, F_4, F_5 and F_6 are functions of t, F_1 and F_2 are functions of both R and t.

B. Small time analytic solution

We seek a small time asymptotic solution when the internal pressure $P = 0$ and decay constant $\lambda = 0$. For a given time t, the solution to the full nonlinear problem satisfies

$$\begin{aligned}
F_1\left[\alpha_1(R,T_{\theta\theta}(R),a,t),T_{\theta\theta}(R)\right] &= 0,\\
F_2\left[T_{\theta\theta}(R),r(R),a,t\right] &= 0,\\
F_{31}\left[\alpha_1(R,T_{\theta\theta}(R),a,t)\right]+F_{32}\left[\alpha_2(R,b)\right]+F_{33}\left[\alpha_3(R,c)\right] &= 0,\\
F_4[c,d] &= 0,\\
F_5[b,c] &= 0,\\
F_6[T_{\theta\theta}(R),a,b,t] &= 0,
\end{aligned}$$

where

$$\begin{aligned}
F_1[\alpha_1,T_{\theta\theta}] &= \alpha^2 Q_1[\alpha]+\int_A^R \frac{dR'}{R'}Q_1[\alpha]-T_{\theta\theta},\\
F_2[T_{\theta\theta},r,a,t] &= \left(a^2+2e^{\nu_2 t}\int_A^R e^{\nu_1 T_{\theta\theta}t}R'dR'\right)^{1/2}-r,\\
F_{31}[\alpha] &= \int_A^B \frac{dR}{R}Q_1[\alpha],\\
F_{32}[\alpha] &= \int_B^C \frac{dR}{R}Q_2[\alpha],\\
F_{33}[\alpha] &= \int_C^D \frac{dR}{R}Q_3[\alpha],\\
F_4[c,d] &= (c^2+D^2-C^2)^{1/2}-d,\\
F_5[b,c] &= (b^2+C^2-B^2)^{1/2}-c,\\
F_6[T_{\theta\theta},a,b,t] &= \left(a^2+2e^{\nu_2 t}\int_A^B e^{\nu_1 T_{\theta\theta}t}R'dR'\right)^{1/2}-b,
\end{aligned}$$

and

$$\begin{aligned}
\alpha_1(R,T_{\theta\theta},a,t) &= \frac{\left(a^2+e^{\nu_2 t}\int_A^R e^{\nu_1 T_{\theta\theta}(R')t}R'dR'\right)^{1/2}}{Re^{\nu_2 t/2+\nu_1 T_{\theta\theta}(R)t/2}}, \quad \text{when } A\leqslant R\leqslant B\\
\alpha_2(R,b) &= \frac{\left(b^2+R^2-B^2\right)^{1/2}}{R}, \quad \text{when } B<R\leqslant C\\
\alpha_3(R,c) &= \frac{\left(c^2+R^2-C^2\right)^{1/2}}{R}, \quad \text{when } C<R\leqslant D.
\end{aligned}$$

Linearizing about the base state $t=0$, $a=A$, $b=B$, $c=C$, $d=D$, $T_{\theta\theta}(R)=0$, $r(R)=R$, the first order variations satisfy the linear system

$$\begin{aligned}
\left[\frac{\delta F_1}{\delta\alpha_1}\frac{\delta\alpha_1}{\delta T_{\theta\theta}}+\frac{\partial F_1}{\partial T_{\theta\theta}}\right]\delta T_{\theta\theta}+\left[\frac{\delta F_1}{\delta\alpha_1}\frac{\partial\alpha_1}{\partial a}\right]\delta a &= -\left[\frac{\delta F_1}{\delta\alpha_1}\frac{\partial\alpha_1}{\partial t}\right]\delta t,\\
\left[\frac{\delta F_2}{\delta T_{\theta\theta}}\right]\delta T_{\theta\theta}+\left[\frac{\partial F_2}{\partial a}\right]\delta a+\left[\frac{\delta F_2}{\delta r}\right]\delta r &= -\left[\frac{\partial F_2}{\partial t}\right]\delta t,\\
\left[\frac{\delta F_{31}}{\delta\alpha_1}\frac{\delta\alpha_1}{\delta T_{\theta\theta}}\right]\delta T_{\theta\theta}+\left[\frac{\delta F_{31}}{\delta\alpha_1}\frac{\partial\alpha_1}{\partial a}\right]\delta a+\left[\frac{\delta F_{31}}{\delta\alpha_1}\frac{\partial\alpha_1}{\partial b}\right]\delta b+\left[\frac{\delta F_{31}}{\delta\alpha_1}\frac{\partial\alpha_1}{\partial c}\right]\delta c &= -\left[\frac{\delta F_{31}}{\delta\alpha_1}\frac{\partial\alpha_1}{\partial t}\right]\delta t,\\
\left[\frac{\partial F_4}{\partial c}\right]\delta c+\left[\frac{\partial F_4}{\partial d}\right]\delta d &= 0, \qquad\qquad (B.1)\\
\left[\frac{\partial F_5}{\partial b}\right]\delta b+\left[\frac{\partial F_5}{\partial c}\right]\delta c &= 0,\\
\left[\frac{\delta F_6}{\delta T_{\theta\theta}}\right]\delta T_{\theta\theta}+\left[\frac{\delta F_6}{\delta a}\right]\delta a+\left[\frac{\partial F_6}{\partial b}\right]\delta b &= -\left[\frac{\partial F_6}{\partial t}\right]\delta t,
\end{aligned}$$

where square parentheses indicate that the term is to be evaluated at the $O(1)$ base solution. Note that terms such as $\left[\frac{\delta F_1}{\delta\alpha_1}\right]$ are actually linearized integral operators and $\alpha(R)\equiv 1$ at the base solution.

The terms in square parentheses are:

$$\begin{aligned}
&\left[\tfrac{\delta F_1}{\delta\alpha_1}\right](\cdot)=Q_1'[1]\left(1+\textstyle\int_A^R\frac{dR'}{R'}\right)(\cdot), && \left[\tfrac{\delta\alpha_1}{\delta T_{\theta\theta}}\right]=0, && \left[\tfrac{\delta F_1}{\delta T_{\theta\theta}}\right]=-1, && \left[\tfrac{\partial\alpha_1}{\partial a}\right]=\tfrac{A}{R^2},\\
&\left[\tfrac{\partial\alpha_1}{\partial t}\right]=-\tfrac{A^2\nu_2}{2R^2}, && \left[\tfrac{\delta F_2}{\delta T_{\theta\theta}}\right]=0, && \left[\tfrac{\delta F_2}{\delta r}\right]=-1, && \left[\tfrac{\partial F_2}{\partial a}\right]=\tfrac{A}{R},\\
&\left[\tfrac{\partial F_2}{\partial t}\right]=\tfrac{\nu_2(R^2-A^2)}{2R}, && \left[\tfrac{\delta F_{31}}{\delta\alpha_1}\right]=Q_1'[1]\textstyle\int_A^B\frac{dR'}{R'}(\cdot), && \left[\tfrac{\delta F_{32}}{\delta\alpha_2}\right]=Q_2'[1]\textstyle\int_B^C\frac{dR'}{R'}(\cdot), && \left[\tfrac{\partial\alpha_2}{\partial b}\right]=\tfrac{B}{R^2},\\
&\left[\tfrac{\delta F_{33}}{\delta\alpha_3}\right]=Q_3'[1]\textstyle\int_C^D\frac{dR'}{R'}(\cdot), && \left[\tfrac{\partial\alpha_3}{\partial c}\right]=\tfrac{C}{R^2}, && \left[\tfrac{\partial F_4}{\partial c}\right]=\tfrac{C}{D}, && \left[\tfrac{\partial F_4}{\partial d}\right]=-1,\\
&\left[\tfrac{\partial F_5}{\partial b}\right]=\tfrac{B}{C}, && \left[\tfrac{\partial F_5}{\partial c}\right]=-1, && \left[\tfrac{\delta F_6}{\delta T_{\theta\theta}}\right]=0, && \left[\tfrac{\partial F_6}{\partial a}\right]=\tfrac{A}{B},\\
&\left[\tfrac{\partial F_6}{\partial b}\right]=-1, && \left[\tfrac{\partial F_6}{\partial t}\right]=\tfrac{\nu_2(B^2-A^2)}{2B}. &&&&
\end{aligned} \qquad (B.2)$$

Since $Q_k[1]=0$ for $k=1,2,3$, solving eq. (B.1) yields the solutions (4.1).

C. Metropolis-Hastings Algorithm for Estimating Credible Intervals

1. Find the minimum of χ^2 (given by Eq. (5.7)) using a routine such as Matlab's `fmincon.m`. Let the minimizer of χ^2 be $\theta^{(0)}\in\mathbb{R}^3$.
2. Set stepsizes $\sigma_1,\sigma_2,\sigma_3$ and initial guess $\theta^{(0)}\equiv(\theta_1^{(0)},\theta_2^{(0)},\theta_3^{(0)})$.
3. For $i=0,1,\ldots,$ numtrials (a specified integer):
4. Generate random increments $\delta\theta\sim\times(\sigma_1N(0,1),\sigma_2N(0,1),\sigma_3N(0,1))$

5. Let $\theta^{(temp)} = \theta^{(i)} + \delta\theta$.

6. Compute $r_{\text{proposed}} = P(\omega|\theta^{(temp)})P(\theta^{(temp)})$ and $r_{\text{current}} = P(\omega|\theta^{(i)})P(\theta^{(i)})$.

7. Let
$$\theta^{(i+1)} = \begin{cases} \theta^{(temp)} & \text{with probability} \quad p = \min(1, r_{\text{proposed}}/r_{\text{current}}), \\ \theta^{(i)} & \text{with probability} \quad 1-p. \end{cases} \tag{C.1}$$

The algorithm produces a sequence $\{\theta^{(i)}\}$, $i = 0, 1, \ldots$ which are guaranteed to be samples from the posterior distribution (5.5). Because the priors for Θ_1, Θ_2 and Θ_3 are compactly supported, $\theta^{(i)} \equiv (\theta_1^{(i)}, \theta_2^{(i)}, \theta_3^{(i)})$ can never leave the domain $[\ell_1, \ell_2] \times [\ell_3, \ell_4] \times [\ell_5, \ell_6]$. In order to perform the large number of trials required for convergence, we ran the algorithm in parallel on a large cluster with each set of runs initialized with $\theta^{(0)}$ and aggregated the results.